A new 3D geological model and structural evolution of the world-class Rio Tinto VMS deposit, Iberian Pyrite Belt (Spain)

A. Martin-Izard, D. Arias, M. Arias, P. Gumiel, D.J. Sanderson, C. Castañon, A. Lavandeira, J. Sanchez

PII: S0169-1368(15)00160-2
DOI: doi: 10.1016/j.oregeorev.2015.06.006
Reference: OREGEO 1534

To appear in: *Ore Geology Reviews*

Received date: 24 February 2015
Revised date: 4 June 2015
Accepted date: 9 June 2015

Please cite this article as: Martin-Izard, A., Arias, D., Arias, M., Gumiel, P., Sanderson, D.J., Castañon, C., Lavandeira, A., Sanchez, J., A new 3D geological model and structural evolution of the world-class Rio Tinto VMS deposit, Iberian Pyrite Belt (Spain), *Ore Geology Reviews* (2015), doi: 10.1016/j.oregeorev.2015.06.006

A new 3D geological model and structural evolution of the world-class Rio Tinto VMS deposit, Iberian Pyrite Belt (Spain).

A. Martin-Izard[a]*, D. Arias[a], M. Arias[a], P. Gumiel[a], D.J. Sanderson[b], C. Castañon[c], A. Lavandeira[d], J. Sanchez[d]

[a]*Department of Geology, Oviedo University, C/Arias de Velasco s/n, E-33005 Oviedo, Spain.*
[b]*Faculty of Engineering and the Environment, University of Southampton, Southampton, SO17 1BJ, United Kingdom.*
[c]*Department of Mines Research and Exploitation, Oviedo University, E-33004 Oviedo, Spain.*
[d]*Emed-Tartessus, La Dehesa S/N, Minas de Rio Tinto, E-21.660 Huelva (España).*

** Corresponding author e-mail: amizard@geol.uniovi.es*

Abstract

A new 3D geological model and structural evolution of the Rio Tinto world-class VMS deposit is presented in this work. The Rio Tinto volcanogenic massive sulfide (VMS) deposit is located in the Spanish segment of the Iberian Pyrite Belt and is hosted by felsic porphyritic volcanic rocks and tuffs. Computer generated 3D modeling of the different orebodies and host rocks has been carried out using data from around 3,000 drill-core logs, allowing us to build 93 cross-sections and 6 plants (both 50 m spacing). This has enabled us to recognize of the geometry and relationships between the mineralization and the earliest Carboniferous transtensional tectonics through the development of an extensional pull-apart basin with two sub-basins separated by the NW-SE trending Eduardo Fault. The sub-basins, Cerro Colorado and San Dionisio, were limited by two E-W strike-slip faults, the Northern and Southern faults, and bounded in the east and west by the NW-SE-trending Nerva and Western faults, respectively. The generated pull-apart basin was first filled by a basaltic magmatism of mantle origin and later, following the deposition of the intermediate complex sedimentary unit, by rhyodacitic volcanic rocks of crustal origin. The evolution of the subsiding basins caused the development of an E-W oriented rollover anticline that affected these filling rocks.

As a result of a counterclockwise rotation of the stress axes, the primitive pull-apart basin evolved into a basin affected by E-W transtensional sinistral shearing. Its northern and southern limits were favorable areas for increased hydrothermal fluid flow, which gave way

to the huge concentration of VMS mineralization located near the limits. The Northern and, to a lesser degree, the Southern extensional faults thus become channel areas for feeding and discharging of the VMS and stockwork ores. The main mineralizing period was related to this stage. Subsequently, during the Variscan transpressional phase, the E-W extensional faults were reactivated as inverse faults, affecting the volcanic sequence of mafic to felsic composition and the intermediate complex sedimentary unit. Fault propagation folds developed above these faults, affecting the massive sulfides, the transition series and the Culm flysch sediments, with buttressing playing a significant role in the geometry of tectonically inverted structures. The VMS mineralization and cupriferous stockworks were folded and dismembered from the original conduits in the volcanic series, and a dextral reactivation of the NW-SE trending faults also developed.

Finally, it should be emphasized that this new 3D geological model is an approach to provide a better insight into the 3D structure of the world-class VMS Rio Tinto deposit and could be a key-point for further studies providing a new tool to increase knowledge of the VMS mineralizations and exploration guidelines elsewerein the IPB.

Keywords: Rio Tinto deposit, 3D modeling, transtensional tectonics, pull-apart basin, VMS, stockwork, Variscan Orogeny.

1. Introduction

The Iberian Pyrite Belt (IPB) extends from Portugal to Spain, covering an area of around 250 km by up to 60 km, located in the South Portuguese Zone (-SPZ-, Fig. 1 A). In its central part, the SPZ contains the greatest known concentrations of volcanic-hosted massive sulfides (VMS) on Earth. The South Portuguese Zone (SPZ), together with the Ossa-Morena Zone (OMZ) and Central Iberian Zone (CIZ) to the north, formed in Devonian-Carboniferous times due to collision with left-lateral transpressional kinematics of Laurentia (SPZ) with Gondwana (OMZ and CIZ) (Oliveira, 1990; Simancas et al., 2003; Mantero et al. 2011).

The IPB contains over 100 massive sulfide and stockwork deposits and many more small prospects (Fig. 1B) (i.e., Pinedo-Vara, 1963; Sáez et al., 1996; Leistel et al., 1998). Over 10 giant (world-class) deposits, with more than 50 million metric tons (Mt) of ore, are hosted by volcanic rocks or associated shales, and were formed as exhalative ores in brine pools on the sea-floor or as filled veins and replacement-style mineralization (e.g., e.g., Solomon et al.,

2002; Tornos, 2006; Gumiel et al., 2010a). The IPB has been estimated to hold a minimum resource of more than 1700 Mt of VMS (Almodovar et al., 1998; Leistel et al., 1998; Sáez et al., 1999; Carvalho et al., 1999; Tornos, 2006). Outstanding among the mines is Rio Tinto, which is the largest deposit in the IPB and has been estimated to have held more than 500 Mt of massive pyrite, complex and stockwork types (Williams et al., 1975; Barriga, 1990; Boulter, 1993; Adamides, 2013).

Figure 1

Recently, the origin of the massive sulfide deposits, several authors (e.g., Oliveira, 1990; Moreno and Gonzalez, 2004; Mantero et al. 2011) invoke transtensional fracturation tectonic process during the early Carboniferous (between 356 and 349 Ma, Tucker et al, 2002), that favored the emplacement of volcanic rocks through the accompanying fractures. Moreover, other authors propose that the whole IPB metallogenic province was formed in rather restricted pull-apart basins within a transpressive Orogeny (Oliveira, 1990; Gumiel et al., 2010a). Although these models are generally accepted and, as is demonstrated by Gumiel et al. (2010a) and Arias et al. (2011), there is clear relationship between fractures and ores, the geometry and relationships between specific deposits and transtensional tectonics are not clearly understood. In fact, a detailed interpretation that explains the structural control during ore formation has not been explained for any deposit up to now.

In all the IPB VMS deposits the presence of fractures/faults, pyrite- and chalcopyrite- rich stockworks, massive sulfides both pyritic and complex, host volcanic and sedimentary rocks, is well known (Williams 1934; Pinedo Vara, 1963; Carvalho et al., 1976; IGME, 1982; Barriga, 1990; Leistel et al., 1994; Leistel et al. 1998, Tucker et al., 2002; Tornos, 2006), but the relationships between these elements and the transtensional tectonics claimed for their genesis in the regional models of the IPB, are not explained in any single deposit.

It should also be emphasized that, after this transtensional period, with the progress of the Variscan Orogeny, the IPB was subjected to transpression (in the sense of Sanderson and Marchini, 1984). Thus, processes during which the mineralization and the associated host-rocks and structures, underwent an intense superimposed deformation, often made recognition of earlier transtensional structures difficult.

Between 2009 and 2013 there was an attempt as part of the ProMine project (FP7 Programme, E.U.), run in Rio Tinto mining district, to carry out 3D semi-regional modelling in a 30x10 km area including Rio Tinto (Díez-Montes et al., in press).

The present work deals with 3D local, detailed modelling of an area of about 6 km^2, exclusively centered in the Rio Tinto deposits and their immediate host rocks, reaching a high level of accuracy in the building and reconstruction of faults and folds. Different drilling surveys performed from 1950 to the last survey carried out by Río Tinto SAL in 2000, have been used to reconstruct the development of the deposits. This involved access to more than 5,000 drill-core logs from Rio Tinto mine, around 3,000 of which (Fig. 2A) have been used in the present study. These allow us a detailed reconstruction of the structure of the deposit through the generation of 93 N-S cross-sections (Fig. 2B), and subsequent 3D modeling, which is presented for the first time in this work. Planes-San Antonio VMS masses are included separately in this 3D reconstruction because the quality and quantity of the data from these orebodies provide less information and also there is a 300 m gap (Fig. 2B) for which less drill-hole data is available between Cerro Colorado and Planes. Nevertheless, the data from the whole area confirm the presence of the so-called Nerva Fault, the stockwork and massive sulfides in Planes and complex massive sulfides in San Antonio which, although not outcropping at the surface, are located approximately at 300 m depth below the Culm slates (see section 5 and Fig. 3).

For this reconstruction, re-logging of these 3,000 boreholes has been carried out in an attempt to unify the criteria used by different geologists in logging operations and thus to establish a coherent geological database. In the computer-generated 3D model we have considered pyritic stockwork to be when the sulfur content is over 20%, and cupriferous stockwork when the copper content is higher than 0.2%. In fact, stockworks are much more broadly extended, but we have set these cut-offs because they are the limits of evaluation criteria.

Finally, we have also highlighted the relationships between transtensional faulting and the resulting basins to the geometry of the stockworks, which has been shown by Gumiel et al. (2010a) and Arias et al. (2011) to be fractal, emphasizing the fact that stockworks have a distinctly mushroom shape from the feeder faults towards the surface.

Figure 2

2. Regional geology

The IPB is part of the Iberian Massif, which resulted from the amalgamation of three continental blocks: the South Portuguese Zone (SPZ), the Ossa Morena Zone (OMZ), and the ensemble of the Central Iberian Zone (CIZ), West Asturian-Leonese (WALZ) and Cantabrian (CZ) zones (Fig. 1A). All of these originated from the fragmentation of a Late Proterozoic megacontinent (Murphy and Nance, 1991). The IPB, which is part of the SPZ, formed as a series of marine basins which developed during the left-lateral transcurrent faulting generated by the oblique subduction and collision of Laurentia with Gondwana during the Variscan (Late Devonian−early Carboniferous; Silva et al., 1990; Oliveira, 1990) and were coeval in time with the presence of a mantle plume (Simancas et al., 2003). These basins were formed within the passive margin of Laurentia, now represented by the South Portuguese zone and adjacent to the continent−continent suture.

The oldest rocks in the IPB (Fig. 1B) are a sequence of late Devonian quartz-rich sandstones and shales (the Phyllite-Quartzite Group, PQ) which were deposited on a stable epicontinental shelf (Schermerhorn, 1971). The overlying Volcanic Sedimentary Complex (VSC) hosts most of the mineralization and is a highly variable unit, up to 1300 m thick, of uppermost Devonian to middle Visean (ca. 356–349 Ma) age (Silva et al., 1990; Tucker et al, 2002; Simancas et al., 2003; Oliveira et al., 2004; Pereira et al., 2007). It is characterized by dacitic–rhyolitic dome complexes and sills, basaltic lava flows and sills, and thick pumice- and crystal-rich felsic volcanoclastic units interbedded with detrital sedimentary rocks, mostly mudstone with some greywacke and sandstone (i.e., Soriano and Martí, 1999). The depositional environment appears to be dominated by submarine mass-flow tuffs as indicated by Schermerhorn (1971). Stratigraphically high in the volcano sedimentary sequence is a horizon, around 10 m thick, of hematitic radiolaria-rich, purple-colored shale with Mn-bearing jasper lenses, which has been used as a local correlation marker in some areas of the IPB (Routhier et al. 1980; Oliveira 1990; Leistel et al., 1998; Soriano and Martí 1999; Carvalho et al., 1999). The VSC is capped by the flysch Group (Culm), consisting of synorogenic turbidites of late Visean to middle-late Pennsylvanian age (Oliveira, 1990).

The earliest Carboniferous (about 360 to 350 Ma) was a transient period characterized by extension and I-type magmatism (Simancas et al., 2003). Abundant bimodal volcanism and

the extensive development of VMS mineralization were mainly emplaced along the fracture zones limiting the different basins (Oliveira, 1990), hitherto not defined on a mine scale. The faults responsible for the crustal thinning and basin formation were developed in a left-lateral transtensional regime in a continental passive margin, and some of these basin-forming faults were reactivated as thrusts during later Variscan shortening (Oliveira, 1990; Gumiel et al., 2010a).

Within this scenario, and on a very large scale controlled by fracture/fault systems, the different VMS deposits developed, the largest ones probably having been controlled by the larger, most active and well-connected faults and fractures developed over an area heated by a mantle plume (Simancas et al., 2003). As described by Gumiel et al. (2010a), most of the massive sulfides are underlain by stockworks hosted within hydrothermally altered rocks. This ore-related hydrothermal alteration predated the regional metamorphism and was caused by the early circulation of modified seawater (Munhá, 1990). Up to the present, most of the well-known stockworks studied seem to have an irregular morphology and are hosted by volcanic rocks that show an irregular zonation, usually with an internal chlorite-rich zone surrounded by a sericitic or propylitic zone. Silicification is a frequent alteration process and carbonatization is also described.

Volcanic rocks mainly occur as shallow intrusions into wet marine sediments with some lava, hydroclastic rocks and volcanogenic sediments in a depositional environment dominated by submarine mass-flow tuffs (Schermerhorn, 1971; Mitjavilla et al., 1997). Most of the basaltic rocks are continental tholeiites, but a few samples show an alkaline affinity. The origin of the basaltic rocks and their diversity of composition are explained by a single mixing model between E-type and N-type-MORB (Mid-Ocean Ridge Basalt) and assimilation of crustal material. Intermediate calc-alkaline and silicic rocks include basaltic andesites, andesites, dacites and rhyolites, the last two being the most abundant. Intermediate and silicic rocks are not related through fractional crystallization, nor is there a relationship between the basaltic and calc-alkaline rocks by the same process (Mitjavilla et al., 1997).

Some authors (Mitjavilla et al. 1997; Leistel et al. 1998) suggest that in the Iberian Pyrite Belt, silicic calc-alkaline magmas were generated on a large scale by the invasion of continental crust by mafic magmas generated in the underlying upper mantle. The diversity of compositions shown by dacites and rhyolites can mainly be explained either by

differences in the composition of the source rocks or by different degrees of partial melting of upper-crust rocks. Andesites, however, formed by the mixing of basaltic magmas and upper-crust material (Mitjavilla et al., 1997; Munhá, 1983).

As indicated by Rosa et al. (2010), the diversity of volcanic lithofacies recognized in different areas of the IPB mainly reflects variations in proximity to source, but also differences in the eruption style. The IPB volcanoes are intra basinal and dominated by felsic lavas/domes that occur at several stratigraphic positions within the volcanic center. Moreover, the pyroclastic units are also abundant and are spatially related to the lavas/domes.

From a structural point of view, the Iberian Pyrite Belt can be considered as a south-verging, thin-skinned, fold and thrust belt that propagated southwards over a mid-crustal basal detachment (Silva et al., 1990; Quesada, 1998, Mantero et al., 2011). This event inverted the previous extensional structures acquired during the initial stages of the collisional process. The Variscan deformation in the SPZ was initiated by the oblique collision between the two (SPZ and OMZ) continental terranes in a transpressional setting. The metamorphic grade is mostly very low, typically prehnite-pumpellyite facies. However, in the northern part of the Iberian Pyrite Belt and near thrusts, deformation is more intense and the rocks are recrystallized within the greenschist facies (Munhá, 1990).

It must be emphasized that the VMS mineralization is related to early Carboniferous fracture/faults with the deposits clustered and localized by these structures. Some early fractures were reactivated during later Variscan thrusting and this may have produced a spatial correlation between thrusting and the location of mineral deposits (Gumiel et al., 2010a; Arias et al., 2011).

3. Geology of the Rio Tinto district study case

Six main geological units, which are roughly coincident with those defined by García Palomero (1980, 1990) and García Palomero et al (1986), were clearly recognized in the drill-core logs (Fig. 3). From the bottom to the top these units are: basaltic rocks (over 250 m thick, with some black slates intercalated), intermediate slates and conglomerates with some interbedded felsic volcanic rocks (up to 40 m thick) acid volcanic rocks (of variable thickness, between 75 m at the western limit, more than 170 m in Corta Atalaya, 140 m

around Eduardo fault and up to 400 m in Cerro Colorado close to the Northern fault, 350m close to the southern fault and between 200 and 300 m in the central zone) hosting at its top the massive-sulfides (always close to the Northern or Southern faults), transition series (around 10 m, up to 30 m) and Culm (syn-orogenic flysch sediments). Affecting the first four groups of rocks are two main types of stockworks, pyritic (over 20% sulfur content) and cupriferous (over 0.2% copper content). In many deposits of the IPB, stockworks act as feeder zones to more massive mineralization (Nehlig et al., 1998).

Figure 3

In the Rio Tinto district, the stockworks comprise a network of interconnected fractures that isolate and partially replace blocks of host rock of variable size. The fractures are filled with quartz and sulfides (mainly pyrite and chalcopyrite) to varying thicknesses. In their deepest parts, stockworks are narrow and formed by thin quartz-sulfide veins in the volcanic rocks (Fig. 4A). These veins become thicker towards the surface. Close to the massive sulfides, most of the stockwork is made up of veins with lesser amounts of strongly replaced volcanic rock (Fig. 4B). Also, towards the surface, the stockwork becomes broader with a mushroom geometry.

In the Rio Tinto area, the stockworks affect the basic unit (basalts), the intermediate unit and the acid volcanic rocks. Within the latter, some levels being more affected than others giving way to different geometries such as those of sections 3800 —Atalaya— and 2750 —Cerro Colorado— (Fig. 5, A and B). Mineralization, hydrothermal alteration and replacement (i.e., silicification, chloritization, sericitization and sulfuration) also infiltrate into the blocks, often along fine fractures.

Figure 4

The Rio Tinto deposit has been described in several papers (Mellado et al., 2006; Gumiel et al., 2010a and references therein) that have proposed that the currently dismembered lenses of massive sulfides formed a large area covering about 4 km^2, with a total estimated tonnage of more than 500 Mt. The underlying stockworks crop out in the Cerro Colorado area, in the core of an anticline verging towards the south, and in Masa San Dionisio—Corta Atalaya, in the sub-vertical southern limb of the anticline (Figs. 3 and 5A, B). The rhyodacitic domes and plugs (Figs. 3 and 6) predate the formation of the stockworks and massive

sulfides, which are capped by the above-mentioned transition series forming a marker horizon in the whole IPB (Tornos, 2006).

Figure 5

The rocks of the Rio Tinto area show intense hydrothermal alteration, with an irregular distribution controlled by the host lithology and syn-sedimentary faults (Leistel et al., 1998, Gumiel et al., 2010a). The shale, polymictic breccia and basalt show a single chlorite-rich zone. The felsic volcanic rocks show a zoned alteration, with a pervasive sericitization that is cross-cut by a later chlorite-rich alteration. Locally, a silica—chlorite-rich alteration zone is found adjacent to the faults. At Cerro Colorado and Corta Atalaya, the alteration around the stockworks is chloritic, with intense silicification. Further from the stockworks, the rocks have a syngenetic sericitic alteration that, in areas near the surface (western part), show kaolinization as a result of weathering (Gumiel et al., 2010a). An important volume of sulfides in Cerro Colorado and minor amounts in Corta Atalaya have developed extensive gossans which were exploited from the sixties to the end of 1998 for gold, whith more than 106 t (3.5 M oz) obtained (García Palomero et al., 1986; Arribas, 1998). In our 3D reconstruction of Rio Tinto we do not take into account the supergene alteration, considering the gossanized stockworks and massive sulfides as part of the deposit.

In the Rio Tinto area it is difficult to differentiate, at the map scale, the domes and lavas from the pyroclastic units related to them. Nevertheless, in the core of the Rio Tinto anticline, rhyodacitic domes and lavas dominate (Figs. 3 and 6), whilst outside this domain, including the Eduardo fault area, pyroclastic tuffs dominate (Garcia Palomero, 1980; Adamides, 2013). Some domes and plugs have been included in the map as part of the felsic sequence, but not in the 3D model because it was not possible to reconstruct them from the drill-core logs.

Figure 6

4. Methodology used in 3D modeling

The use of 3D models facilitate the understanding of surface and subsurface geology is well-established by several authors (i. e., Houlding, 1994; Lemon and Jones, 2003; Calcagno et al., 2008; Kaufman and Martin, 2008; Maxelon et al., 2009; Gumiel et al., 2010b; Wang et al., 2013).

The 3D model was generated using 3D GeoModeller© (www.geomodeller.com), which was developed by BRGM (French Geological Survey; Lajaunie et al., 1997; Calcagno et al., 2002). In this software, lithological units are described as a pseudostratigraphic pile, intended to image the geology and structural relationships as closely as possible. Compared with other existing 3D solid modeling approaches (e.g. Boissonnat, 1988; Bertrand et al., 1992), a major feature of this tool is that the 3D description of the geological space is achieved through a potential field formulation in which geological boundaries are iso-potential surfaces, and their dips are represented by gradients of the potential. The model is built in a georeferenced system and uses (i) a digital elevation model (DEM), (ii) a simplified geological map, sections and plans (lithological contact information) and (iii) fractures/faults measured within the different units (local gradient information).

Figure 7

The 3D modeling involved several steps for the processing of data according to their type (Fig. 7 A to C):

First step. Incorporation of the digital elevation model into ArcGIS 10.1© software (ASCII format) to model the topographic surface. Acquiring, compiling and standardizing the geological information and borehole data. The sources of the datasets are:

A)) Topography 1:10,000 scale from the Andalusian Institute of statistic and mapping, Digital Elevation Model (DEM in ASCII format, 2009), and PNOA ortho-image of Rio Tinto area from ©Instituto Geográfico Nacional (2014).

B) Geological surface data from the authors. The use of the geological reports from the Rio Tinto staff, drill-hole logs and the works from Williams (1934), García Palomero (1980) Gumiel et al. (2010) were very useful.

C) Reports and geological information of old underground workings. This information was very useful in helping to obtain an accurate shape of the massive sulfides and stockworks and a precise location of faults where the drill-hole data were scarce, as for example, at the south fault.

D) From the 5,000 existing drill-hole logs, after a short examination we selected around 3,000 that contain valuable lithological or structural information and we re-log these drill-holes as mentioned above in the introduction section. For the 3D model we

established a coherent geological database with the 7 units and 3 mineralization types, as indicated previously.

Second step. Hand drawing of 93 N-S vertical cross-sections, spaced at 50 m intervals, using the boreholes data projected on the sections (Fig. 2). Based on these, another 6 horizontal sections from the 450 m level to 200 m have also been drawn, both at 1:2,000 scale. The methodology followed is well known in geology, often being applied to mineral exploration and mining (i.e., McKinstry, 1970; Marjoribanks, 2010).

The sections and plants have been georeferenced and digitalized to produce the XYZ coordinates of each contact between the units and mineralized bodies defined in step 1, and the geological structures. All this digitized information has been stored in a Geodatabase created in ArcGis 10.1©, and the correctness of the topological relationships between the digitized elements has been checked.

Third step. Importation of all geological contacts, fault intersections and DEM from the Geodatabase to Geomodeller© using a script developed by us that allows the data format transformation. Geological surface models were built by contact and dip vectors derived from the sections and DEM. Geological subsurface objects were validated by the large borehole data at depth.

The use of sections that were built directly from drill-hole data permits us to use them as depth constraints.

5. Geological characteristics of the different elements in the 3D geological model: Stockworks and rollover geometry.

Two main E—W trending fault zones have been characterized in the 3D geological model of Rio Tinto mine (Figs. 8, 9 and 10, Appendix 1 and 2), namely the Northern and the Southern Fault zones. They are subparallel and approximately 1 km apart. Moreover, these two faults are crosscut by the NW—SE trending Eduardo Fault zone, which dissects both E—W faults in two sections. The first, approximately 3 km in length, and lying to the East of the Eduardo Fault, gives way to the Cerro Colorado area, which ends in the Nerva Fault zone. The other section, lying farther west, is approximately 1 km in length and is limited by the Western Fault zone. This sector corresponds to the San Dionisio-Corta Atalaya area (Figs. 3, 8, 9, 10

and 11). The Western fault zone is outside the 3D-modeled area. These fault zones delimit two sub-basins; the Cerro Colorado sub-basin, of 3x1 km to the east of Eduardo Fault, and the San Dionisio sub-basin, of 1x1 km westward of Eduardo Fault (Figs. 8, 9, 10 and 11). This fault is barren from a metallogenic point of view, as was previously mentioned by Williams (1934) and Pinedo Vara (1963). The San Dionisio sub-basin is displaced around 100 m to the north as a result of the dextral kinematics of the Eduardo Fault zone (Fig. 3, see section 6).

Figure 8

Figure 9

Figure 10

The geometry and trace of the mentioned faults are well reflected in the Residual Bouguer Anomaly map (gravity survey, Fig. 12), within which the whole Rio Tinto area corresponds to an E—W-trending positive anomaly that terminates abruptly and is bent at the western and eastern ends by the Western and Nerva fault zones respectively. Two narrow areas can be observed; the western one corresponding to the Eduardo Fault zone and the eastern one to a locally defined NNW—SSE fracture. The gravity map agrees with the pull-apart basin that gives way to the Rio Tinto mineralized area.

Figure 11

In Cerro Colorado there is a narrow area between the pyrite rich stockwork of Salomon and the rest of Filon Norte to the west. The so-called 1800 fault lies within this narrow area. Also, to the east, close to Argamasilla mass, is located the Argamasilla N—S fault (Figs. 3 and 12). The 1800 fault is seen in the open pit but is not included in the 3D sections because it is difficult to follow in the drill core logs and in the N—S sections. Locally, these NW—SE faults affected the Culm sediments and in some cases small amounts of massive sulfides appear as olistoliths (Fig. 13) at the bottom of the Culm slates, as can be seen in the western limb of Eduardo fault or in the area of the Argamasilla fault (Fig. 3 and 12).

Figure 12

Figure 13

It is noteworthy that the Northern Fault is almost vertical whilst the Southern Fault initially dips around 80° to the north but its dip becomes gentle with depth (Fig. 8A, B, C and Fig. 9A)

and probably intersec the Northern Fault at a relatively small dip angle. The southern Fault is therefore antithetic to the Northern Fault, and is developed within the formation of a rollover anticline. Other minor fractures are developed subparallel or conjugate to the previously mentioned faults, outstanding among them being the so-called middle fault (Fig. 3), the NW—SE 1800 fault, the N—S Argamasilla fault and the NE—SW fault-set in Cerro Colorado, which may be conjugate structures to the Eduardo fault.

An important contribution of this 3D model to the knowledge of the structural evolution of the area is the modeling of an E—W-trending rollover anticline favored by the Northern and southern extensional faults (Figs. 8, 9, 10 A to C, and 14 A). This structure displays (Fig. 14 A) a turtle shape (Rouby et al., 2002), which originated by both vertical shear (Verrall, 1981; Gibbs, 1983, 1984) and bending associated with slip on the synthetic fault (Northern Fault) and on the antithetic (Southern Fault), similar to models described by McClay (1990) and Imber et al. (2003).

Figure 14

The subsiding area evolves into a transtensional graben, bounded by the two normal faults (Northern and Southern fault) and becoming progressively more asymmetric, with the faults probably connecting at depth. These faults bounding the sub-basins are related to a pull-apart structure and are favorable areas for the intrusion of igneous rocks, especially in transtensional zones. This magmatism in the Rio Tinto area started with basaltic volcanism that marked the beginning of the transtensional process related to the formation of the pull-apart basins. After the basaltic volcanism and the deposition of the intermediate unit, the acid volcanism commences with the emplacement of rhyolite—dacite domes and the generation of lavas and abundant submarine mass-flow tuffs, cinerites and the volcanism characteristic of the area (Garcia Palomero, 1980). The variation in thickness of the acid volcanism previously mentioned are in agreement with the rollover geometry, being thicker close to the Northern and Southern faults and thinner in the axis of the rollover and close to the Eduardo fault. The role of the E—W trending faults is critical in explaining the genesis, location and structure of the VMS and cupriferous stockworks of the Rio Tinto district. The 3D model suggests that hydrothermal circulation and discharge are highly focused and localized along these syn-sedimentary faults, acting as feeder channels to the hydrothermal fluids (Figs. 8, 9, 10 A to C, and 14 B).

In all cases, the stockworks are located between the Northern and Southern faults and most of the massive sulfides are also located between these two faults, although small masses of VMS locally may occur beyond these fault limits. In certain areas the hydrothermal fluids discharge onto the seafloor producing substantial volumes of massive sulfides These may remain on the stockworks (as at Filon Norte, Filon Sur, San Dionisio and Planes) or small masses may be transported when the syn-sedimentary basins are filled up by the VMS. In the latter case,the VMS that seals and extends beyond the Northern and Southern faults (as at Filon Norte and San Dionisio).

In the case of the San Antonio complex sulfides, the eastern end of the Rio Tinto structure, the syn-sedimentary displacement of the VMS mass is more significant, extending beyond the Nerva Fault zone in the east (Figs. 3 and 10 B, C), probably as a consequence of the filling up of the syn-sedimentary basins.

Although most of the stockworks are located in the acid volcanic series, a few are hosted in the intermediate unit and in the basic volcanic rocks. When they were formed, the roots of the stockworks were located in the master E—W trending faults. In the deeper parts, the stockworks were subvertical and relatively narrow, and towards the surface became broader while near to the top of the system they became almost horizontal (mushroom-shape). This geometry is now noticeable in the northern sector of Cerro Colorado area where the stockworks are developed from the domes to the abundant volcanoclastic material, frequently following bedding planes or other rock discontinuities (Figs. 8, 9 and 10 A to C).

The Northern and Middle Faults and the formation of stockworks and VMS mineralization were active after the deposition of the acid volcanic unit, ceasing their activity before the deposition of the transition series that seals them. All massive sulfide orebodies are located on the top of the acid volcanic series, and in some areas, such as the southern part of San Dionisio mass, the syn-sedimentary basins were filled up by the VMS that were displaced over the faults and fossilized them. During the Variscan transpressional phase the Culm sedimentary sequence was deposited and folded, and the E-W extensional faults were reactivated as contractional structures operating as reverse faults (Fig. 14 C), affecting the basic and acid volcanic rocks and the intermediate unit. Shortening was accomplished by folding and reverse reactivations of faults, which propagate upwards developing fault-related folds that affect the massive sulfides (see Figs. 11 and 14 C), the transition series and

the Culm (Fig. 15) as shown in the computer-generated 3D model. During this compressive stage the rollover is tightened and its southern flank becomes more vertical, developing an anticline verging to the south (Fig. 14 C). Also, the two sub-basins associated with the rollover and limited by the Northern (Cerro Colorado) and Southern faults (San Dionisio) are folded as synclines (Figs. 9 B and 14 C) and the faults become more vertical. The massive sulfides deposited in these two sub-basins, which seal the extensional faults, were also folded (Figs. 5, 8, 9, 10, 11 and 14 C).

Figure 15

6. Tectonic evolution of the Rio Tinto area based on the generated 3D model

The computer-generated 3D model has been used to explain the tectonic evolution of the Rio Tinto area and its implications for the VMS mineralizations; two clearly differentiated structural stages can be distinguished (Fig. 16):

1) **Pre-Variscan transtensional phase**. This transtensional stage, active during the earliest Carboniferous and associated bimodal magmatism, is critical to explain the VMS deposits of the Rio Tinto area. An early stage starts with the development of a pull-apart having two sub-basins (Cerro Colorado and San Dionisio –Atalaya sub-basin, Fig. 16 A) limited by the NW-SE trending Eduardo Fault Zone and of two sinistral strike-slip fault zones of the same orientation, the Nerva and Western Fault zones, bounding the eastern and western areas respectively. These faults overlap and generate a transtensional zone of interaction limited by two extensional E-W trending faults (the Northern and Southern Faults) bounding the pull-apart. This geometrical pattern can be explained by a NW-SE shortening (σ_1) and a resultant NE-SW extension (σ_3) (Fig. 16 A). In addition, as has been shown (i.e. Connolly and Cosgrove, 1999; Drew 2006, Zhang et al., 2008), in a transtensional pull-apart the most favorable areas for increased fluid flow and highest concentration of mineralization are located near the boundaries, such as the areas delimited by red ellipses in Fig. 16.

Figure 16

Later, as a result of a counterclockwise rotation of the stress axes (around 30°), the shortening (σ_1) becomes WNW-ESE and the extension (σ_3) roughly N-S. At this stage the Northern and Southern Faults are dominantly extensional, forming a conjugate pair with the Southern Fault being antithetic and linked at depth to the Northern Fault, localizing extension and promoting the formation of the rollover anticline (Fig. 14 A). The resulting extensional basins were first filled by the basaltic magmatism of mantle origin and then, after the deposition of the intermediate unit sediments, by the latter acid volcanism, all of them being folded in a rollover anticline structure (Fig. 14 A). At this time the Eduardo Fault Zone starts to assume relevance since it probably represents a basement tectonic structure with sinistral strike-slip kinematics (Fig. 16 A, B and C).

Likewise, the favorable areas (red ellipses) for promoting fluid flow and mineralization increase on both sides of the basins in the Northern and Southern extensional faults, becoming areas for the feeding and discharge of the VMS and copper stockwork mineralizations (Figs. 14 B and 16 B, C). We also emphasize the fact that the ENE-WSW orientation of the Cu-stockworks roughly coincides with the orientation of tension cracks parallel to the (σ_1) direction (Fig. 16 C).

E-W trending transtensional sinistral shearing (Fig. 16 C) becomes active and continues over time as a result of a counterclockwise rotation of the stress axes (25°-30°), the shortening (σ_1) being ENE-WSW trending and the extension (σ_3) NNW-SSE trending.

2) **Variscan transpressional phase**. This stage of deformation developed in the Visean orogenic phase, persisting until the end of the Carboniferous. During transpression (in the sense of Sanderson and Marchini, 1984), prolonged E-W trending shear with sinistral kinematics was developed. This produced southerly-directed folding and thrusting, with reactivation of the early basin bounding faults. It also produced dextral reactivation of the NW-SE trending faults (Fig. 14 C and 16 D), with new sinistral NE-SW trending faults (synthetic Faults 1 and 2), both systems at a high angle to the main E-W trend of the IPB. WNW-ESE to E-W oriented folds plunging eastward and a reverse component in the NW-SE faults (i.e. Eduardo Fault) is developed. The transpressional nature of the Variscan deformation on a regional scale has been mentioned by several authors (i.e. Quesada, 1998; Soriano and Casas, 2002; Silva and Pereira, 2004; Simancas et al., 2006; Gumiel et al., 2010a;

Arias et al., 2011), however, till now, it has not been established on the local scale, nor had it been used to explain the overall tectonic evolution of the Rio Tinto area.

As was suggested by Arias et al. (2011), the role of the NW-SE trending faults, in particular the Eduardo Fault Zone in Rio Tinto, when connected with the E-W trending extensional faults generates dilation zones favorable for mineral concentration (Figs. 14 B and 16 C, D).

As shown in the 3D model, the Variscan folding in the area (Figs. 5, 8, 9 and 10, Appendix 1 and 2) is reflected by an anticline and two synclines plunging to the East, and the VMS mineralization and cupriferous stockworks are folded and dismembered from the original conduits (Northern Fault) in the acid volcanic series (Figs. 14 C and 16D).

Above the Northern Fault, a fault-related fold is developed (Figs. 8 B, C, 9 A, B and 14 C). The geometry of this folded sequence is easily observed in the transition series, unconformable with the VMS mineralization and the rest of the sequence. This geometrical pattern was controlled by the lower series (acid, intermediate and basic) buttresses in the footwall block of the Southern Fault. This suggests that buttressing (in the sense of Bayley et al., 2002) of the lower series plays a significant role in the geometry of tectonically inverted structures and the partitioning of deformation in the area. Therefore, during this transpressional phase, reactivation of the syn-sedimentary faults is critical (Figs. 14 C and 16 D).

The NE-SW trending oblique compression (σ_1) also favors the development of an inverse component in some faults, such as the Eduardo Fault, that increase the strike-slip fault movement with dextral kinematics. During transpression, an approximate estimate of shortening is around 30-40%, based on the proposed 3D model. Finally, the orientation of the extension (σ_3) is NW-SE, leading to a progressive counter-clockwise rotation and tectonic inversion.

7. Discussion

The general structure of Rio Tinto results from two main periods of deformation. The first is largely transtensional and, after the deposition of slates and quartzites (the PQ formation) in a stable continental shelf, produced localized extension and basin development, with associated volcanism and the development of the Volcanic Massive Sulfide deposits. The second was transpressional, producing reactivation and compression during the Variscan Orogeny produced by the oblique convergence of Gondwana and Laurentia.

In the Rio Tinto area, the early stage began with the development of a pull-apart with two sub-basins (Cerro Colorado and Atalaya) through two NW-SE trending sinistral strike-slip fault zones, the Nerva and Western fault zones, bounding the eastern and western areas respectively. These faults overlap and generate a transtensional pull-apart zone of interaction limited by two extensional E-W trending faults (the Northern and Southern Faults).

The localization of this extension in the Rio Tinto area, facilitates a process of mantle decompression with the intrusion of large volumes (over 250 m thick) of basaltic rocks of mantellic origin (Mitjavilla et al. 1997), favored by the extensional faults bounding the pull-apart. Upon the emission of the basaltic rocks, the infilling of the basin continues with slate sediments (black shales) and intercalated basalts and tuffs forming the so-called intermediate unit (García-Palomero, 1980), sometimes with a conglomeratic appearance as defined by Williams (1934). During this transtensional process with the development of these pull-apart basins, partial melting of crustal rocks occurred, leading to the subsequent emplacement of the acid volcanic sequence, thus developing the characteristic bimodal volcanism of the area.

The emplacement of magmas of this acidic volcanic sequence was favored by the E-W trending extensional faults bounding the transtensional basins. This acid volcanism leads to thicker acidic tuff sequences, mostly in the Cerro Colorado and San Dionisio areas, into which some rhyodacitic plugs subsequently intrude. Most of the recognized rhyodacitic plugs are located on or in the vicinity of the extensional E-W trending faults bounding the basins.

During this stage, the maximum aperture of the transtensional pull-apart occurs and a rollover anticline is developed. In fact, the Northern fault corresponds to a deep synthetic fault that initially favors the formation of a rollover anticline affecting both volcanism (basic and acid) and the intermediate unit, and channels most of the acid volcanism and, later, hydrothermal activity (Figs 9 A and 14 A).

This activity was of less impact in the Southern fault. This may explain why Cerro Colorado stockwork and Filon Norte massive sulfides constitute the main mineralized area at Rio Tinto.

According to the proposed structural model (Fig. 16), during this phase, as a result of a counterclockwise rotation of the stress axes, the primitive pull-apart basin evolved into a basin affected by an E-W trending transtensional sinistral shearing. The main mineralizing period was probably related to this stage after the emplacement of the rhyodacitic plugs, with the development of kilometric-scale geothermal convective cells generated around the basin, in accordance with the models proposed by Sato (1972, 1977), Lambert and Sato (1974) and Turner and Campbell (1987). These cells were controlled by the E-W trending faults on a large scale, and by the rhyodacitic plugs at local scale. The formation of the different mineralized structures must have been directly related to this long term hydrothermal activity, which also explains the low dispersion of lead isotopic geochemistry (Marcoux, 1998). The extensional tectonics seems to be essential to homogenize throughout hydrothermal cells lead isotopes (García-Sansegundo et al, 2014; Palero-Fernandez et al. 2015).

It is also noteworthy that the stockwork at Cerro Colorado trends slightly obliquely to the Northern fault (Fig. 10A), this direction coinciding with the orientation of tension cracks parallel to the (σ_1) during this stage (Fig. 16 C).

Dilation zones located on E-W trending faults promoted connectivity between fractures and cracks of volcanic rocks, thereby focusing the hydrothermal flow from deep areas to the surface, and thus producing well-connected stockworks, as has been demonstrated (Gumiel et al., 2010a; Arias et al, 2011). The stockworks are hosted in the volcanic sequence and are all located in the vicinity of the Northern and Southern faults, from which the roof of the basic rocks, the transition and the middle and upper part of the acid series mineralize. From the master faults, the stockwork mineralization penetrates the bedding planes defined in the volcanic rocks and the intermediate unit, developing the above mentioned mushroom geometry. As seen in Figures 8, 9, 10 and 14, these stockworks are narrow and vertical in the deeper parts, opening up towards the surface. In the deeper areas, the network of veins is narrower and dominates the volume of rock, while toward the surface vein thickness progressively increases and veins clearly dominate over replaced host rock fragments, which are strongly altered (chloritized, silicified and sulfurized). Finally, in certain areas hydrothermal fluid was discharge onto the seafloor, producing substantial volumes of VMS mineralization that may remain above the stockworks (i.e. Filon Norte, Filon Sur, San

Dionisio and Planes) or suffer transport with displacement of small masses that seal and surpass the Northern and Southern faults in Filon Norte and San Dionisio (Figs. 8 and 9). However, in the case of the San Antonio deposit (east of Cerro Colorado), the syn-sedimentary displacement of the massive sulfides after the filling of the basin is significant, spreading eastwards over the Nerva Fault zone (Fig. 10 B, C).

Moreover, the NW-SE fault systems play a minor role from the point of view of the mineralization. These faults only appear to accommodate the geometry of the above-mentioned basins and are only associated with minor mineralized veins.

During this transtensional stage, the transition series is deposited covering all the previous mentioned rocks. It represents the final volcanic sediments, several meters thick, which is also a guide level for the IPB (Leistel et al. 1998, Soriano and Marti, 1999, Tornos, 2006).

Later on, during the main Variscan transpressional phase, the Culm sedimentary sequence was deposited and the E-W extensional faults were inverted. For example, the Eduardo fault placed Cerro Colorado sub-basin above the San Dionisio mass. In some places, these NW-SE trending faults affect the Culm sediments and on some occasions fragments of massive sulfide (olistoliths) can slid into the bottom of the Culm slates (i.e. Argamasilla fault, Fig. 13). These faults move as inverse faults, and propagate up as faults-related folds affecting the massive sulfides, the transition series and the Culm (Figs. 5, 8, 9, 10 and 15). During this compressive stage the rollover is tightened and the VMS mineralization of the two sub-basins (Cerro Colorado and San Dionisio) was folded, sealing the extensional faults, (Figs. 5, 8, 9 and 10, Appendix 1 and 2).

The structural model proposed here is coincident in some aspects with those of Neves Corvo (Relvas et al., 2006), the other supergiant deposit of the IPB (Fig. 1 B). This area is farther south than Rio Tinto (Fig. 1 B), hence the Variscan tightening is less, possibly with better preservation of the original transtensional structure. At Neves, where the IPB trend is NW-SE, the SW-NE section (perpendicular to the general trend, see Fig. 3 from Relvas et al., 2005) through Graça and Corvo presents two main faults, the northern being near vertical and the southern dipping around 45° to the NE. Both faults seem to define a similar basin to those proposed here for Rio Tinto. It should also point out that all the stockworks are close to, or between these two faults, and that the massive sulfides are located mostly between the faults. Moreover, the thickness of the Neves Formation increases to the north of the

southern fault and the same happens with the massive sulfides that disappear rapidly to the south. In fact, these two faults probably define a syn-sedimentary subsiding basin in the interior of which the main mineralized structures develop similarly to Rio Tinto.

8. Conclusions

A new 3D geological model and structural evolution of the Rio Tinto world-class VMS deposit is presented in this work. A computer generated 3D reconstruction of the different orebodies and host rocks has been carried out using data from around 3,000 boreholes generating 93 cross-sections with 50m spacing. The resulting geological model has a resolution of ~3 m and includes the exploited mineralization above the present topographical profile as well as the distribution of the VMS and stockwork mineralizations that remains to be mined.

This new 3D geological model leads to a new understanding of the development of the VMS deposits at Rio Tinto and their relationship to the Variscan evolution of Iberia. We provide an interpretation of the geometry and relationships between the mineralization and the earliest Carboniferous transtensional tectonics.

The development of an extensional pull-apart with two sub-basins separated by the NW-SE trending Eduardo fault. The sub-basins, Cerro Colorado and San Dionisio, were limited by two E-W trending faults, (the Northern and Southern faults), and bounded eastward and westward by the NW-SE trending Nerva and Western faults respectively.

As a result of a counterclockwise rotation of the stress axes, the primitive pull-apart basin evolved into a basin affected by E-W trending extensional faults. The formation of subsiding basins caused the development of an E-W trending rollover anticline affecting these filling rocks. We suggest also how these structures evolved, the main structural, magmatic, sedimentary and hydrothermal processes related to them resulting the Rio Tinto deposit. The generated pull-apart were first filled by a basaltic magmatism of mantellic origin and then, after the deposition of the intermediate unit, by a rhyodacitic volcanism of crustal origin. Its northern and southern limits were favorable areas for increased fluid flow and hydrothermalism, producing a huge concentration of mineralization located near the limits, mainly the Northern and, to a lesser degree, the Southern faults becoming channel areas for

feeding and discharge of the VMS and stockwork ores. The main mineralizing period was related to this stage.

At the end of the Carboniferous, the Variscan orogeny produced compression (sinistral transpression) of the IPB. The massive sulfides, the transition series and Culm were all extensively folded and thrust. The early transtensional structures were overprinted with many of the basin-bounding normal faults being inverted and the rollover anticline was tightened. Buttressing mechanism can play a significant role during inversion. The VMS mineralization and cupriferous stockworks were folded and dismembered from the original conduits in the volcanic series, and a remarkable dextral reactivation of the NW-SE trending faults also developed.

Finally, this new contribution to the knowledge of this area of world relevance, based on real data, and the resulting computer-generated 3D geological model of the Rio Tinto district can open new possibilities for prospectivity of the VMS and stockwork mineralizations at the IPB. The geometry and relationships between mineral deposits and the structural evolution at different scales should be carefully studied with special emphasis placed on the transtensional (extensional) processes to explain the origin of these types of mineralization and their prospectivity. In accordance with the proposed model, a new interesting area could be the South fault to the east of the Eduardo fault, because the “Filon Sur” massive sulfides and stockwork could have developed a syncline structure, as happens in Corta Atalaya, but this structure has not been found. As this area is very close to the South fault, it could have been displaced or tectonized during the Variscan shortening and buttressing deformation.

Acknowledgements

The authors wish to thank EMED Tartessus for the drill-core logs and gravimetric data provided. The authors also wish to thank Angelo Farci and Mario Zapico (EMED Tartesus) and Luis Quintana (University of Oviedo) for their help and comments, which greatly improved this manuscript. We are grateful to three anonymous reviewers for their comments and discussion that notably increase the clarity and quality of the paper. We want also to thank

the historical staff of the Minas de Rio Tinto Department of Geology for their drill core logs and contribution to the knowledge of this unique area of world relevance.

References

Adamides, N.G. 2013. Rio Tinto (Iberian Pyrite Belt): a world-class mineral field reopens. Applied Earth Science (Trans. Inst. Min. Metall. B), 122: 1-15.

Almodovar, G.R., Saez, R., Pons, J.M., Maestre, A., Toscano, M., and Pascual, E., 1998, Geology and genesis of the Aznalcollar massive sulfide deposits, Iberian Pyrite Belt, Spain: Mineralium Deposita, v. 33, p.111–136.

Arias, M.; Gumiel, P., Sanderson, D.J., Martin-Izard, A., 2011. A multifractal simulation model for the distribution of VMS deposits in the Spanish segment of the Iberian Pyrite Belt. Comput. Geosci. 37, 1917–1927.

Arribas, A., 1998. Los yacimientos de oro asociados con las monteras limoníticas de la Faja Pirítica Ibérica. Bol. Geol. Min. 109, 9–15.

Barriga, F.J.A.S., 1990. Metallogenesis in the Iberian Pyrite Belt. In: Dallmeyer, R.D., Martinez García, E. (Eds.), Pre-Mesozoic Geology of Iberia. Springer Verlag, pp. 369–379.

Bayley, C.M., Giorgis, S., Coiner, L., 2002. Tectonic inversion and basement buttressing: an example from the central Appalachian Blue Ridge province. J. Struct. Geol. 24, 925–936.

Bertrand, P., Dufour, J.F., Francon, J., Lienhardt, P., 1992. Modélisation volumique à base topologique, Actes MICAD92, Vol. 1. Hermès: Paris, 59–74.

Boissonnat, J.D., 1988. Shape reconstruction from planar cross-sections. CVGIP. Graphical Models and Image Processing 44, 1–29.

Boulter C. A. 1993. Rio-Tinto Guaymas comparisons: super-giant mineralization in an ancient sill-sediment complex. Geology 21: 801-804

Calcagno, P., Martelet, G., Gumiaux, C., 2002. Apport de la modélisation géométrique 3D a' l'interprétation géologique du complexe de Champtoceaux (massif armoricain). 19e'me RST, Nantes, p. 79 (abstract).

Calcagno, P., Courrioux, G., Guillen, A., Chiles, J.P., 2008. Geological modelling from field data and geological knowledge. Part I. modelling method coupling 3D potentialfield interpolation and geological rules. Physics of the Earth and Planetary Interiors 171, 147–15. Carvalho, Dl., Conde,

L., Hernández Enrile, J., Oliveira, V., Schermerhorn, LJG., 1976. Livro-guia das excurso es geolôgicas Faixa Piritosa Ibérica. III Reuniao de Geologia do Sudoeste do Maciczo Hespérico da Penînsula Ibérica, Huelva-Beja, 1975, Comun. Serv. Geol. Port LX, pp. 271–315.

Carvalho, D., Barriga, F., Munhá, J., 1999. Bimodal siliciclastic systems: the case of the Iberian Pyrite Belt. Rev. Econ. Geol. 8, 375– 408.

Connolly, P., Cosgrove, J., 1999. Prediction of static and dyinamic fluid pathways within and around dilational jogs. In: McCaffrey, K.J.W., Lonergan, L. & Wilkinson, J.J. (Eds.), Fractures, Fluid Flow and Mineralization. Geological Society, London, Special Publications 155, pp. 105–121.

Díez-Montes, A., García Crespo, J., Ayala, C., García Lobón, J.L., Sánchez-García, T., Rey, C., Bellido, F., Rubio, F., Mediato, J.F., Tornos, F. (in press) 3D reconstruction of known and unknown geological mineralized bodies in SW Iberia Mining Belt. In: Weihed, Pär (Ed.), 3D, 4D and predictive modelling of mineral belts: European resources under cover. ISBN 978-3-319-17428-0, in press. Drew, L.J., 2006. A Tectonic Model for the Spatial Occurrence of Porphyry Copper and Polymetallic Vein Deposits-Applications to Central Europe. Scientific Investigations Report 2005-5272, U.S. Geological Survey, 36 p.

García Palomero, F., 1980. Caracteres geológicos y relaciones morfológicas y genéticas de los yacimientos del Anticlinal de Riotinto. Instituto de Estudios Onubenses “Padre Marchena”. Excma. Diputación Provincial de Huelva, 264 p.

García Palomero, F., 1990. Río Tinto deposits. Geology and geological models for their exploration and ore reserves evaluation. In: Sulphide deposits - their origin and processing, Inst Institute of Mining and Metallurgy Min Metal, Springer Netherlands, pp. 17–35.

García Palomero, F., Bedia Fernández, J.L., García Magariño, M., y Sides, E.J., 1986. Nuevas investigaciones y trabajos de evaluación de reservas de gossan en Minas de Rio Tinto. Bol. Geol. Min. XCVII-V, 82–102.

García-Sansegundo, J., Martin-Izard, A., Gavaldà, J., 2014. Structural control and geological significance of the Zn–Pb ores formed in the Benasque Pass area (Central Pyrenees) during the post-late Ordovician extensional event of the Gondwana margin. Ore Geol. Rev. 56, 516–527.

Gibbs, A.D., 1983. Balanced cross-section construction from seismic sections in areas of extensional tectonics. Balanced Cross Sections and Their Geological Significance 5, 153–160.

Gibbs, A.D., 1984. Structural evolution of extensional basin margins. J. Geol. Soc. London 141, 609–620.

Gumiel, P., Sanderson, D.J., Arias, M., Roberts, S., Martín-Izard, A., 2010a. Analysis of the fractal clustering of ore deposits in the Spanish Iberian Pyrite Belt. Ore Geol. Rev. 38, 307–318.

Gumiel, P., Arias, M., Martín-Izard, A., 2010b. 3D geological modelling of a polyphase deformed pre-Variscan IOCG mineralization located at the southeastern border of the Ossa Morena Zone, Iberian Massif (Spain). Geol. J. 45, 623–633.

Houlding, S.W., 1994. 3D Geoscience Modeling-Computer Techniques for Geological Characterization. Springer-Verlag, Berlin, Germany, pp. 1–6.

IGME, 1982. Síntesis Geológica de la Faja Pirítica del SO de España. IGME, Madrid. 106 pp.

Imber, J., Childs, C., Nell, P.A.R., Walsh, J.J., Hodgetts, D., Flint, S., 2003. Hanging wall fault kinematics and footwall collapse in listric growth fault systems. J. Struct. Geol. 25, 197–208.Kaufmann, O., Martin, T., 2006. 3D geological modelling from boreholes, cross-sections and geological maps, application over former natural gas storages in coal mines. Comput. Geosci. 34, 278–290.

Lajaunie, C., Courrioux, G., Manuel, L., 1997. Foliation fields and 3D cartography in geology: principles of a method based on potential interpolation. Math. Geol. 29, 571–584.

Lambert, I.B., Sato, T., 1974. The Kuroko and associated ore deposits of Japan: A review of their features and metallogenesis. Econ. Geol. 69, 1215–1236.

Leistel, J. M., Bonijoly, D., Braux, C., Freyssinet, P., Kosakevitch, A., Leca, X., Lescuyer, J. L., Marcoux E., Milési, J.P., Piantone, P., Sobol, F., Tegyey, M., Thiéblemont, D., Viallefond, L., 1994. The massive sulphide deposits of the South Iberian Pyrite Province: geological setting and exploration criteria. BRGM, 234, 236 pp.

Leistel, J.M., Marcoux, E., Thieblemont, D., Quesada, C., Sánchez, A., Almodóvar, G.R., Pascual, E., Sáez, R., 1998. The volcanic-hosted massive sulphide deposits of the Iberian Pyrite Belt. Review and preface to the special issue. Miner. Deposita 33, 2–30.

Lemon, A.M., Jones, N.L., 2003. Building solid models from boreholes and user- defined cross-sections. Computers & Geosciences 29, 547–555.

Marcoux, E. 1998. Lead isotope systematics of the giant massive sulphide deposits in the Iberian Pyrite Belt. Miner. Deposita 33, 45–58

Marjoribanks, R., 2010. Geological Methods in Mineral Exploration and Mining. Springer-Velag, Berlin, Germany. 233 p.

Mantero, E. M. Alonso-ChavesF. M. Garcia-Navarro, E. Azor, A., 2011. Tectonic style and structural analysis of the Puebla de Guzman Antiform (Iberian Pyrite Belt, South Portuguese Zone, SW Spain). In: Poblet, J. and Lisle R.J. (Eds.), Spec. Publ. Geol. Soc. London 349, 203–222.

Maxelon, M., Renard, P., Courrioux, G., Brandli, M., Mancktelow, N., 2009. A workflow to facilitate three-dimensional geometrical modelling of complex poly-deformed geological units. Comput. Geosci., 35 (3), 644–658.

Mcclay, K.R., 1990. Extensional fault systems in sedimentary Basins - a review of analog model studies. Mar. Pet. Geol. 7, 206–238.

McKinstry, H.E. (1970). Geología de minas. Ed. Omega. Barcelona, Spain. 671 p.

Mellado, D., Clavijo, E.G., Tornos, F., Conde, C., 2006. Geologia Y estrutura de la Mina de Rio Tinto (Faja Pirítica Ibérica, España). Geogaceta 40, 231-234.

Mitjavilla, J., Marti, J., Soriano, C., 1997. Magmatic evolution and tectonic setting of the Iberian Pyrite Belt volcanism. J. Petrol. 38, 727–755.

Moreno, C., Gonzalez, F. 2004. Zona Sudportuguesa: Estratigrafía. In: Vera, J. A. (Ed.), Geología de España. SGE-IGME, pp. 201–205.

Munhá, J. 1983. Hercynian magmatism in the Iberian pyrite belt. In: Lemos de Souza J, Oliveira JT (eds) The Carboniferous of Portugal. Mem Serv Geol Port 29: 39±81

Munhá, J., 1990. Metamorphic evolution of the South Portuguese/ Pulo do Lobo Zone. In: Dallmeyer, R.D., Martínez García, E. (Eds.), Pre-Mesozoic Evolution of Iberia. Springer Verlag, pp. 363–368.

Murphy, J.B., Nance, R.D., 1991. A supercontinent model for the contrasting character of Late Proterozoic orogenic belts. Geol. 9, 469–472.

Nehlig P, Cassard D, Marcoux E (1998) Geometry and genesis of feeder zones of massive-sulphide deposits: constraints from the Rio Tinto ore deposit (Spain). Miner. Deposita 33: 137-149

Oliveira, J.T., 1990. South Portuguese Zone: introduction. Stratigraphy and synsedimentary tectonism. In: Dallmeyer, R.D., Martínez García, E. (Eds.), PreMesozoic Geology of Iberia. Springer Verlag, pp. 333–347.

Oliveira, J.T., Carvalho, P., Pereira, Z., Pacheco, N., Korn, D., 2004. Stratigraphy of the tectonically imbricated lithological successions of the Neves-Corvo mine region, Iberian Pyrite belt. Implications for the regional basin dynamics. Mineralium Deposita 34, 422-436.

Palero-Fernandez, F., Martin-Izard, A., Zarzalejos Prieto, M., Mansilla-Plaza, L., 2015. Geological context and plumbotectonic evolution of the giant Almadén Mercury Deposit. Ore Geol. Rev. 64, 71–88.

Pereira, Z., Matos, J., Fernandes, P., Oliveira, J.T., 2007. Devonian and Carboniferous palynostratigraphy of the South Portuguese Zone, Portugal - An overview. Comunicasoes Geológicas 94, 53-79.Pinedo Vara, I., 1963. Piritas de Huelva (su historia, minería y aprovechamiento). Ed. Summa, Madrid, 1003 pp.

Quesada, C., 1998. A reappraisal of the structure of the Spanish segment of the Iberian Pyrite Belt. Miner. Deposita 33, 31–44.

Relvas, J.R.M., Barriga, F.J.A.S., Ferreira, A., Noiva, P.C., nelson Pacheco, N., Barriga, G. 2006. Hydrothermal Alteration and Mineralization in the Neves-Corvo Volcanic-Hosted Massive Sulfide Deposit, Portugal. I. Geology, Mineralogy, and Geochemistry. Econ. Geol. 101, 753-790.

Rosa, C. J.P., McPhie, J., Relva, J.M.R.S., 2010. Type of volcanoes hosting the massive sulfide deposits of the Iberian Pyrite Belt. J. Volcanol. Geotherm. Res. 194, 107–126.

Rouby, D. Raillard, S., Guillocheau, F., Bouroullec, R., Nalpas, T., 2002. Kinematics of a growth fault/raft system on the West African margin using 3-D restoration. J. Struct. Geol. 24, 783–796.

Routhier P, Aye F, Boyer C, Lecolle M, Moliére P, Roger G, Picot P., 1980. La ceinture sud-ibérque à amas sulfurés dans sa partie espagnole mediane. Bur. Rech. Géol. Minière Mém 94, 1–265.

Sáez, R., Almodóvar, G.R., Pascual, E., 1996. Geological constraints on massive sulphide genesis in the Iberian Pyrite Belt. Ore Geol. Rev. 11, 429– 451.

Sanderson, D.J., Marchini, D.R., 1984. Transpression. J. Struct. Geol, 6 (5), 449-458.

Sato, T., 1972. Behaviors of ore-forming solutions in sea water. Min. Geol. 22, 31– 42.

Sato, T., 1977. Kuroko deposits: Their geology, geochemistry and origin. In: Volcanic processes in ore genesis. Spec. Publ. Geol. Soc. London 7.

Schermerhorn, L. J. G., 1971. An outline stratigraphy of the Pyrite Belt. Bol. Geol. Min. 82-84, 239–268.

Silva, J.B., Oliveira, J.T., Ribeiro, A., 1990. Structural outline of the South Portuguese Zone. In: Dallmeyer, R.D., Martínez García, E. (Eds.), PreMesozoic Geology of Iberia. Springer Verlag, pp. 348– 362.

Silva, J.B., Pereira, M.F., 2004. Transcurrent continental tectonics model for the Ossa-Morena Zone Neoproterozoic–Paleozoic evolution, SW Iberian Massif, Portugal. Int. J. Earth Sci. (Geol. Rundsch.) 93, 886–896.

Simancas, J.F., Carbonell, R., González Lodeiro, F., Perez Estaún, A., Juhlin, C., Ayarza, P., Kashubin, A., Azor, A., Martínez Poyatos, D., Ruiz Almodóvar, G., Pascual, E., Sáez, R., Expósito, I., 2003. Crustal structure of the transpressional Variscan Orogen of SW Iberia: SW Iberia deep seismic reflection profile (IBERSEIS). Tectonics 22, 1962–1974.

Simancas, J. F., 2004. Zona Sudportuguesa. In: Vera, J. A. (Ed.), Geología de España. SGE-IGME, pp. 199–222.

Solomon, M., Tornos, F., Gaspar, O., 2002. A possible explanation for many of the unusual features of the massive sulfide deposits of the Iberian Pyrite Belt. Geology 31, 87-90.

Soriano, C., Marti, J., 1999. Facies analysis of volcano-sedimentary successions hosting massive sulfide deposits in the Iberian Pyrite Belt, Spain. Econ. Geol. 94, 867–882.

Soriano, C., Casas J.M., 2002. Variscan tectonics in the Iberian Pyrite Belt, South Portuguese Zone. Int. J. Earth Sci. (Geol. Rundsch.) 91, 882–896.

Tornos, F., 2006. Environment of formation and styles of volcanogenic massive sulfides: the Iberian Pyrite Belt. Ore Geol. Rev. 28, 259–307.

Tucker, B. C. Yuri, A.E. Pascual, E., 2002. U–Pb Geochronology of VMS mineralization in the Iberian Pyrite Belt. Miner. Deposita 37, 684–703.

Turner, J.S., Campbell, I.H., 1987. Temperature, density and buoyancy fluxes in black smoker plumes, and the criterion for buoyancy reversal. Earth Planet. Sci. Lett. 86, 85-92.

Verrall, P., 1981. Structural Interpretations with Applications to North Sea Problems, Course Notes. Joint Association of Petroleum Exploration Courses (JAPEC), London.

Wang, G., Pang, Z., Boisvert, J., Hao, Y., Cao, Y., Qu, J., 2013. Quantitative assessment of mineral resources by combining geostatistics and fractal methods in the Tongshan porphyry Cu deposit (China). J. Geochem. Explor. 134, 85–98.

Williams, D., 1934. The geology of the Rio Tinto mines, Spain. Trans. Inst. Min. Metall. 43, 593–678.

Zhang, Y., Schaubs, P. M. Zhao, C. Ord, A., Hobbs, B. E., Barnicoat A. C., 2008. Fault-related dilation, permeability enhancement, fluid flow and mineral precipitation patterns: numerical models. In: Wibberley, C. A. J., Kurz, W., Imber, J., Holdsworth, R. E. and Collettini, C. (Eds.), The Internal Structure of Fault Zones: Implications for Mechanical and Fluid-Flow Properties. Spec. Publ. Geol. Soc. London 299, 239–255.

Figure captions

Figure 1. A) The zones of the Iberian Massif, CZ: Cantabrian Zone. WALZ: West Asturian-Leonese Zone. CIZ: Central Iberian Zone. OMZ: Ossa Morena Zone. SPZ: South Portuguese Zone. **B)** Geological scheme of the South Portuguese Zone with the location of the main massive sulfide deposits in the IPB, including the Rio Tinto world-class deposit. The geological base is from (Leistel et al. 1998; Simancas 2004; Mantero et al., 2011, and modified by the authors).

Figure 2. A) Location of the 3,000 utilized boreholes from different surveys in Cerro Colorado and Corta Atalaya with the DEM of the area. Information provided by EMED Tartesus. **B)** Location of 93 N-S cross-sections generated based on the carefully study and re-logged of the drill cores used for building up the 3D model presented in this work.

Figure 3. Geological map of the Rio Tinto district, including San Dionisio, Cerro Colorado and Planes orebodies obtained from the 3D geological model and field mapping. The location of the rhyodacitic plugs is approximate.

Figure 4. Two representative aspects of the stockwork mineralization: **A)** Deepest part of the stockwork made up by narrow sulfide veins in rhyodacites. **B)** Close to the surface and near to the massive sulfides, the sulfides prevailing over rock fragments (Cerro Colorado open-pit).

Figure 5. Two representative geological sections of the Rio Tinto deposit: A) Section 3800 Corta Atalaya and B) Section 2700 Cerro Colorado (the same legend as in Figure 3). Both sections have been selected from the 93 sections generated from drilling data. Each section was built using data from the drill core where they intersect the section surface. In the figure are added the drill number (from the Emed Tartesus data base) and its spatial position in the section. **Figure 6.** Rhyodacitic plug in the northwestern part of Cerro Colorado.

Figure 7. Organigram of the methodology carried out to generate the 3D geological model of the Rio Tinto deposit. For explanation, see text.

Figure 8. Different perspectives of the computer-generated 3D geological model of the Rio Tinto VMS deposits (same legend as in Fig. 3). **A)** General view, from SE, of the whole modeled area showing the Cu-stockwork mineralization (light green), the pyritic stockwork

of Salomon and the VMS orebodies (red). Notice the rollover anticline plunging 35°-40° towards east well expressed in the intermediate unit (blue). **B)** View, from SE, of the Cerro Colorado and Corta Atalaya open pits on the orthoimage of the area. Notice the rollover anticline bounded by the Northern and Southern Faults, well expressed in both the intermediate unit (blue) and the transition series (light blue). **C)** A similar panoramic view oriented from SE, and four representative sections have been included in order to facilitate the visualization of the 3D model. Notice both the disposition of the VMS orebodies and the Cu-stockwork mineralization (light green). This view includes the mineralization exploited in both open pits.

Figure 9. A) A detail of the 3-D geological model (eastern view). Notice both the geometry of the VMS mineralization (red) and the disposition of the pyritic (dark green) and the Cu-stockworks (light-green) with a mushroom shape on the rollover anticline. This view includes the exploited mineralization above the present topographical section to enhance the geometry of the rollover anticline. See also the geometry and disposition of the pyritic stockwork close to the vertical Northern Fault (light yellow) and the Filon Sur VMS mineralization close to the Southern Fault (blue). See section 5 for explanation. **B)** General view, from SW, of the Corta Atalaya and Cerro Colorado open pits on the orthoimage of the area. Notice both the disposition of the VMS mineralizations (Filon Norte and San Dionisio-Filon Sur) and the Cu-stockwork mineralization (light green) scattered on the rollover anticline. **C)** View from below, from SE direction, enhancing the geometry of the VMS mineralizations, the Cu-stockwork (light green) and the pyritic stockwork (dark green), showing the existing mineralization below the surface that remains unexploited.

Figure 10. A) Zenith panoramic view of the rollover anticline bounded by the Northern and Southern Faults, well expressed in the intermediate unit (blue) with some folds plunging eastward. Notice both the geometry of the VMS orebodies (red) and the disposition of the pyritic (dark green) and the Cu-stockworks (light-green) scattered on the rollover anticline. The dextral kinematics of the Eduardo Fault can be observed in this view. **B)** Partial view of the eastern area of the 3D model to observe the disposition of the Planes-San Antonio VMS mineralization plunging towards east over the pyritic stockwork (dark green) and the acid unit (light yellow) spreading over the Nerva Fault. Notice the end of the rollover anticline plunging around 35°-40° eastward well expressed in the intermediate unit (blue). Three

representative sections have been included to facilitate the visualization of the 3D model. **C)** A similar view to the previous but below the surface including the exploited mineralization above the present topographical section. Notice the disposition of the Planes-San Antonio VMS mineralization plunging to the east (See section 5 for explanation).

Figure 11. Mapping of the Atalaya open-pit over a current photocomposition and based on field data. The mapping of the lithological units is consistent with the computer-generated 3D model, showing the hydrothermal alteration of the acid and basic volcanic rocks, the Cu-stockwork and folds in the VMS mineralization of San Dionisio mass.

Figure 12. Proposed structural model on the Residual Bouguer Anomaly map, based on the gravity survey of the Rio Tinto area. (Source of the gravity data: EMED Tartesus).

Figure 13. Boulder of massive sulfides into the Culm slates in the eastern side of the Argamasilla fault (see Figure 12 for location of this fault).

Figure 14. Idealized scheme showing the evolution of the rollover anticline; **A)** Extensional stage favored by the Northern and Southern extensional faults with the generation of a rollover anticline, originated by both vertical shear and bending associated with slip on the synthetic fault (Northern Fault) and on the antithetic (Southern Fault). **B)** Diagram showing the critical role of the Northern and Southern Faults to explain the genesis, location and structure of the VMS and cupriferous stockworks of Rio Tinto. **C)** Diagram showing a later transpressional phase. Shortening generates folding of the volcano-sedimentary sequence, the VMS mineralization and cupriferous stockworks which are dismembered from the original conduits (Northern Fault) in the acid series. Reactivation of the Southern Fault as a reverse fault is also observed.

Figure 15. Folds developing a sub-vertical axial plane cleavage in the Culm slates over the Southern fault at Corta Atalaya open-pit.

Figure 16. Idealized diagram showing four stages of the structural model proposed for the Rio Tinto VMS deposit. **A)** Pre-Variscan transtensional phase. An early stage starts with the development of a pull-apart with two sub-basins (Cerro Colorado and Atalaya) and two E-W trending sinistral strike-slip fault zones (the Nerva and Western Fault zones) bounding the pull-apart. **B)** Prolonged transtensional phase. As a result of a counterclockwise rotation (around 30°), the shortening direction (σ_1) becomes WNW-ESE and the extension (σ_3)

roughly N-S. The red ellipses are favorable areas for promoting fluid flow and mineralization. **C)** E-W trending transtensional sinistral shearing becomes active and continues over time as a result of a counterclockwise rotation (25°-30°) of the stress axes. At this stage the highest concentration and discharge of mineralization occurs. **D) Variscan transpressional phase**. During transpression, prolonged E-W trending shear with sinistral kinematics is developed, producing a remarkable dextral reactivation of the NW-SE trending faults acting as antithetic faults (i.e. Eduardo Fault). For explanation see section 6.

Table 1.

Summary of the main features related to the tectonic evolution of the Rio Tinto area based on the generated 3D model.

1) Pre-Variscan Transtensional period
a) Transtensional pull-apart stage
- Basaltic magmatism
- Acid volcanism with rhyodacitic plugs
b) Transtensional sinistral shearing stage
- Development of a rollover anticline structure
- Main mineralizing moment producing stockworks and VMS mineralization
- Transition series deposition
2) Variscan Transpressional period
a) Transpressional sinistral shearing stage
- Culm sedimentary sequence deposition
- Folding and thrusting with inversion of E-W trending extensional faults
- Buttressing

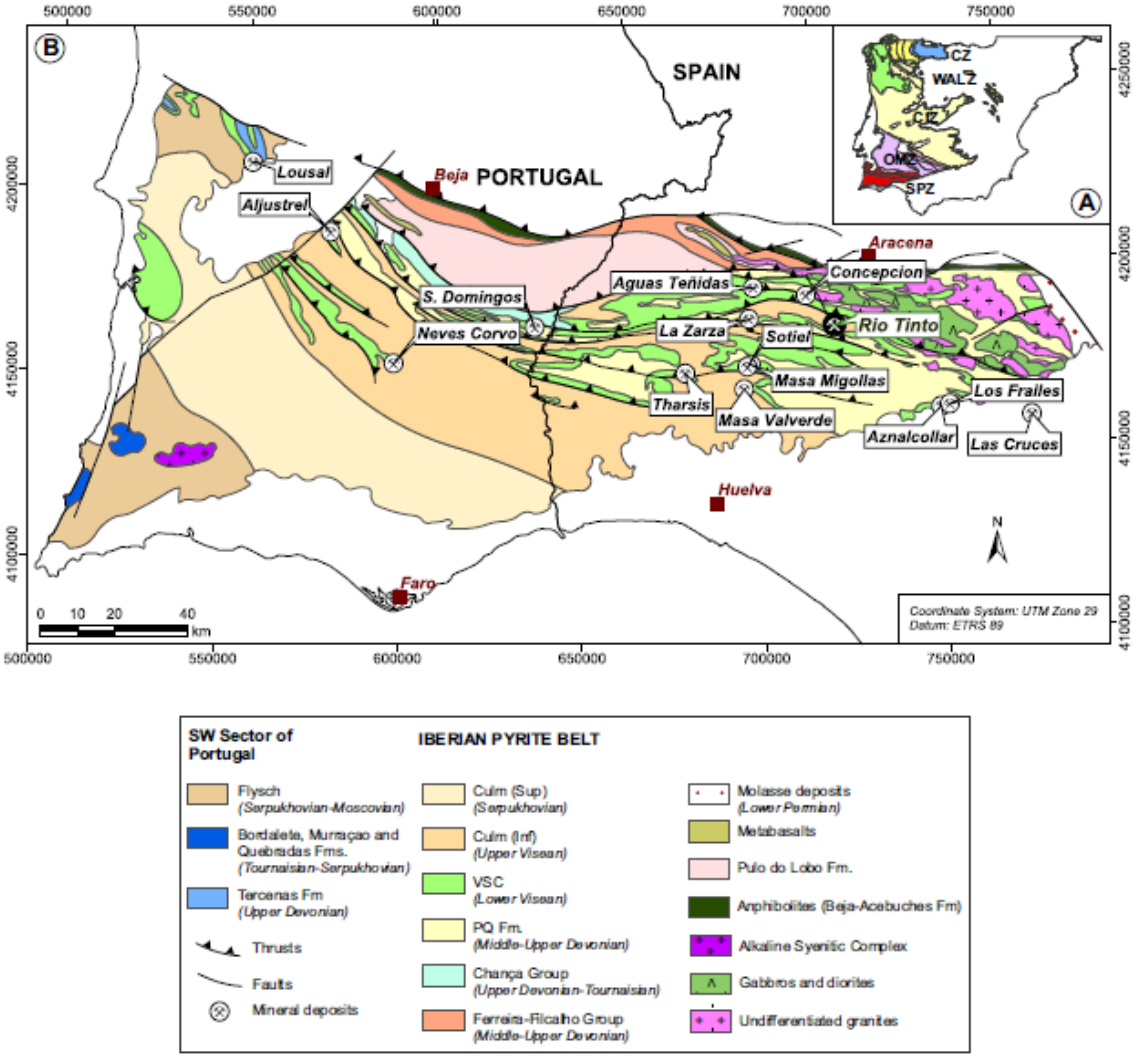

Figure 1

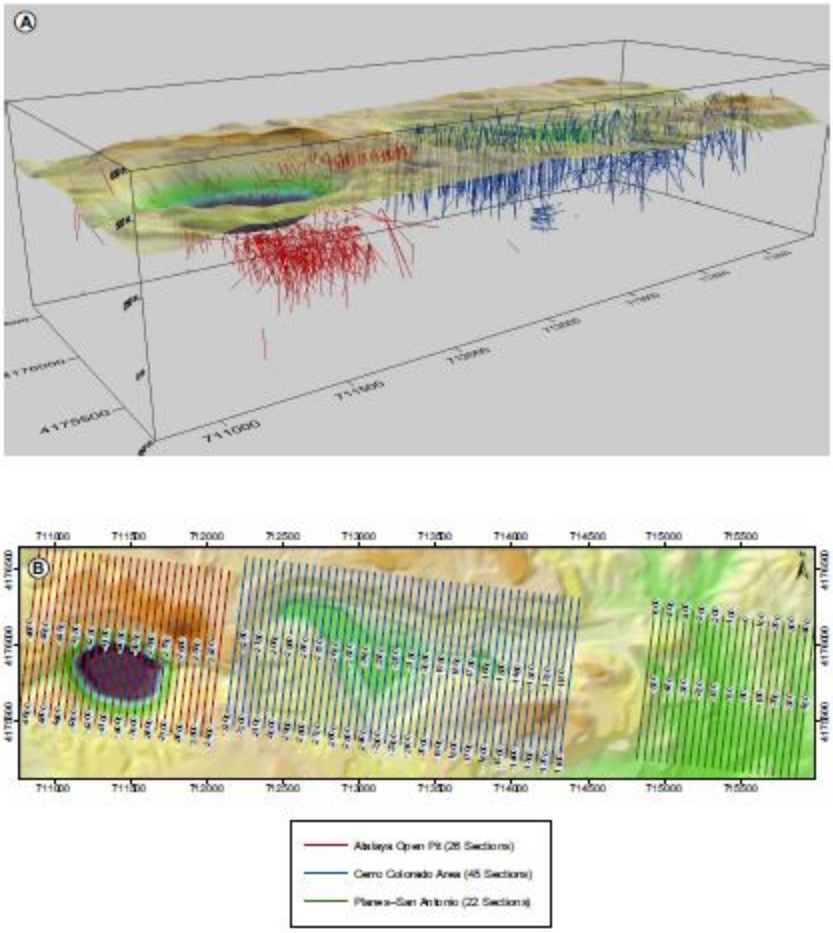

Figure 2

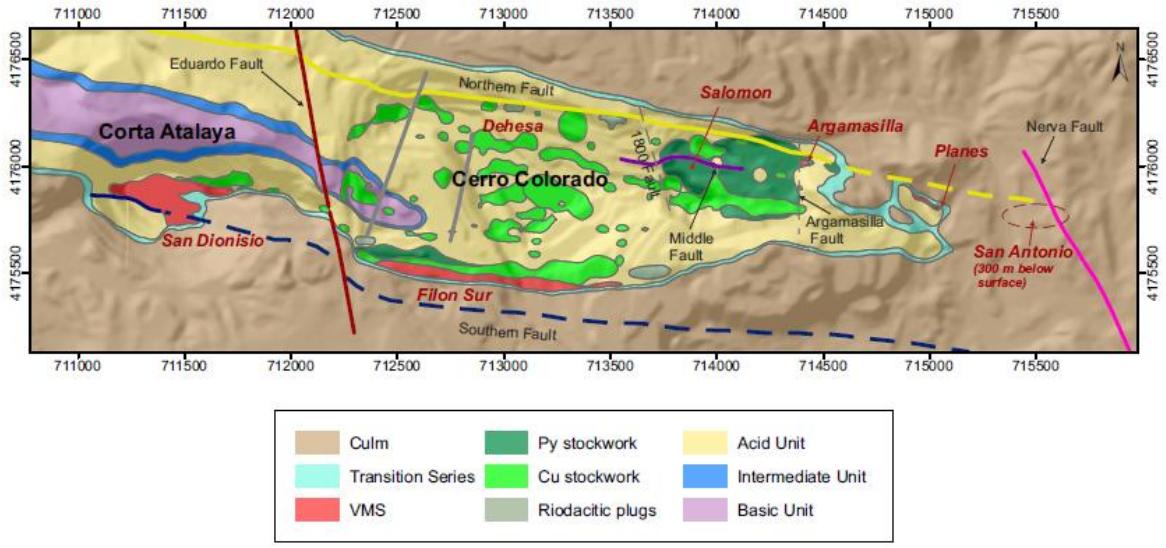

Figure 3

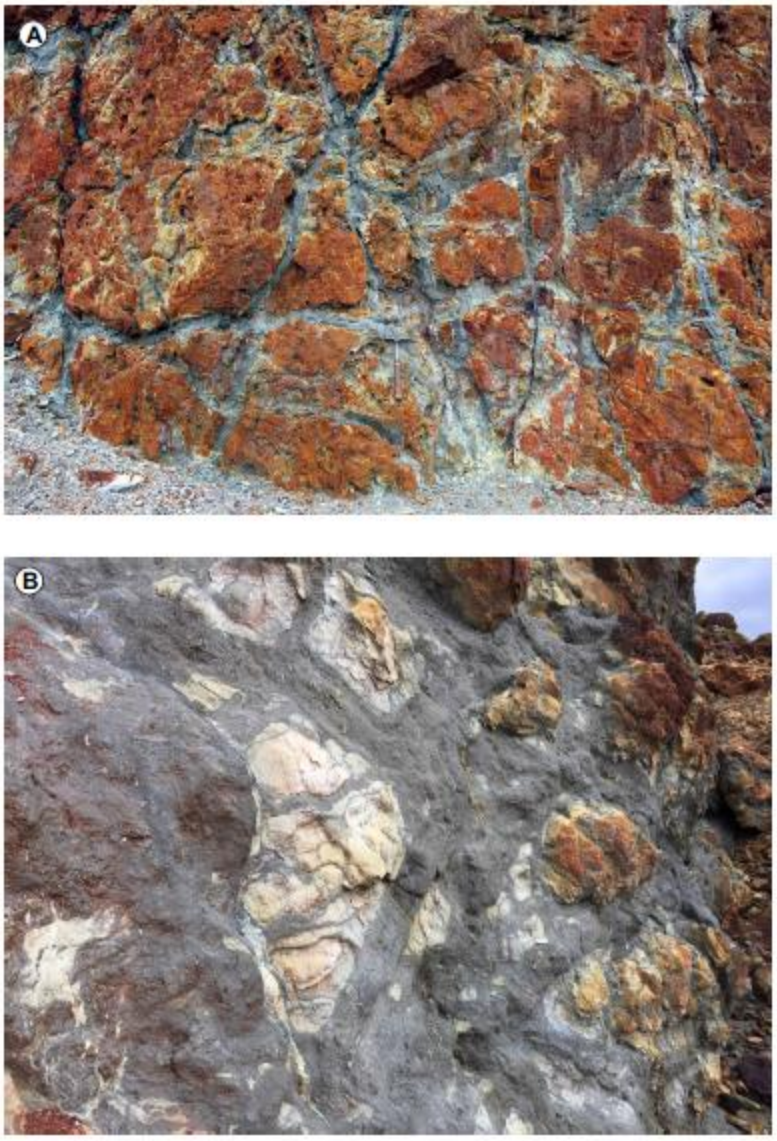

Figure 4

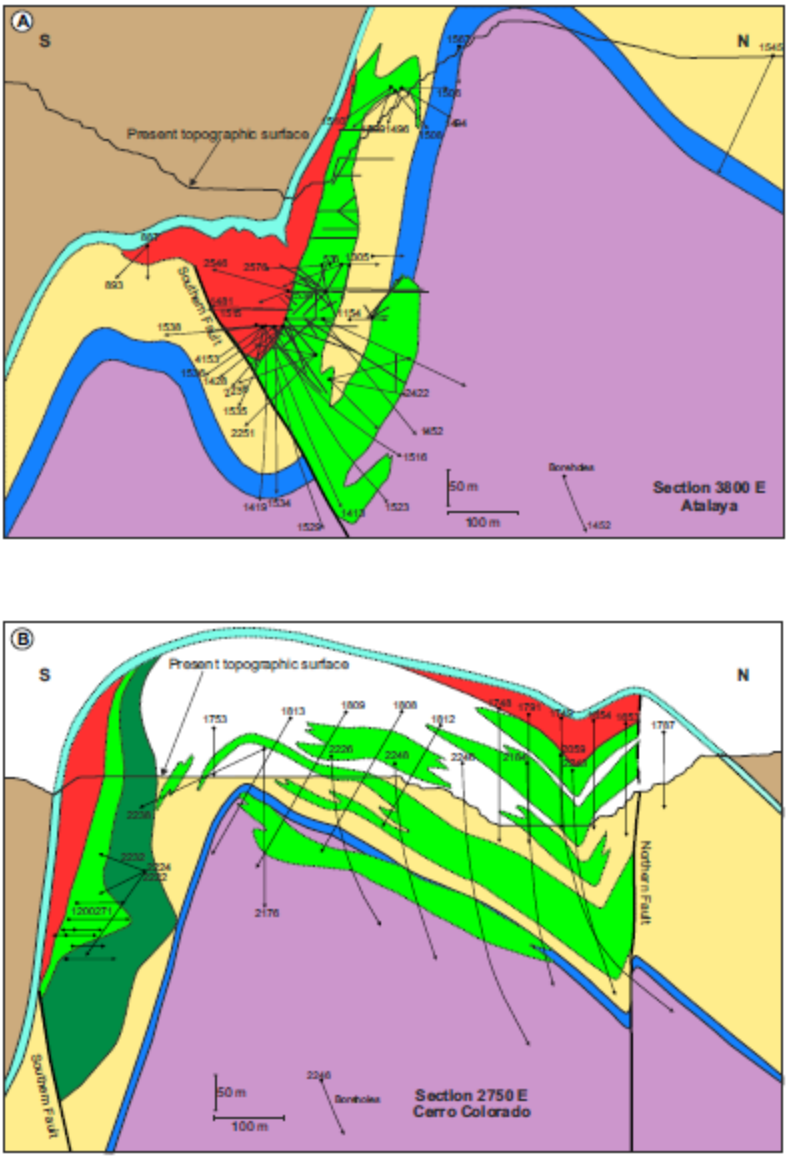

Figure 5

Figure 6

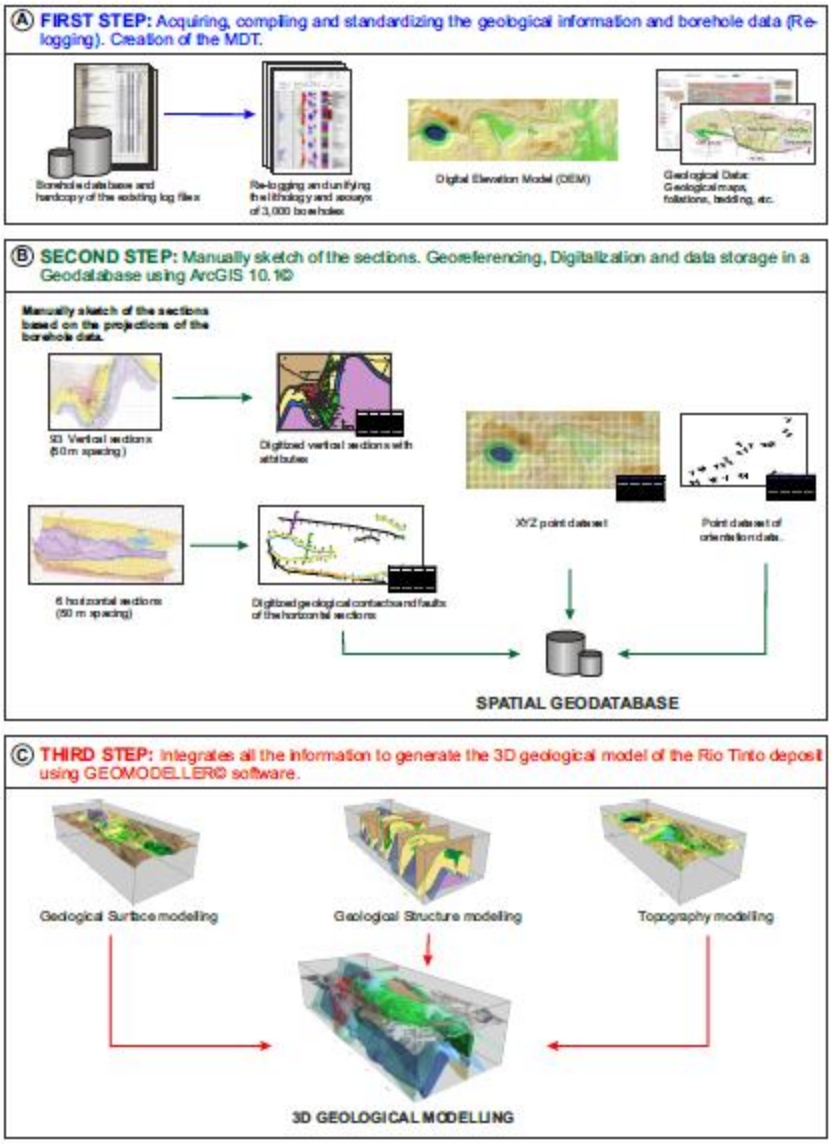

Figure 7

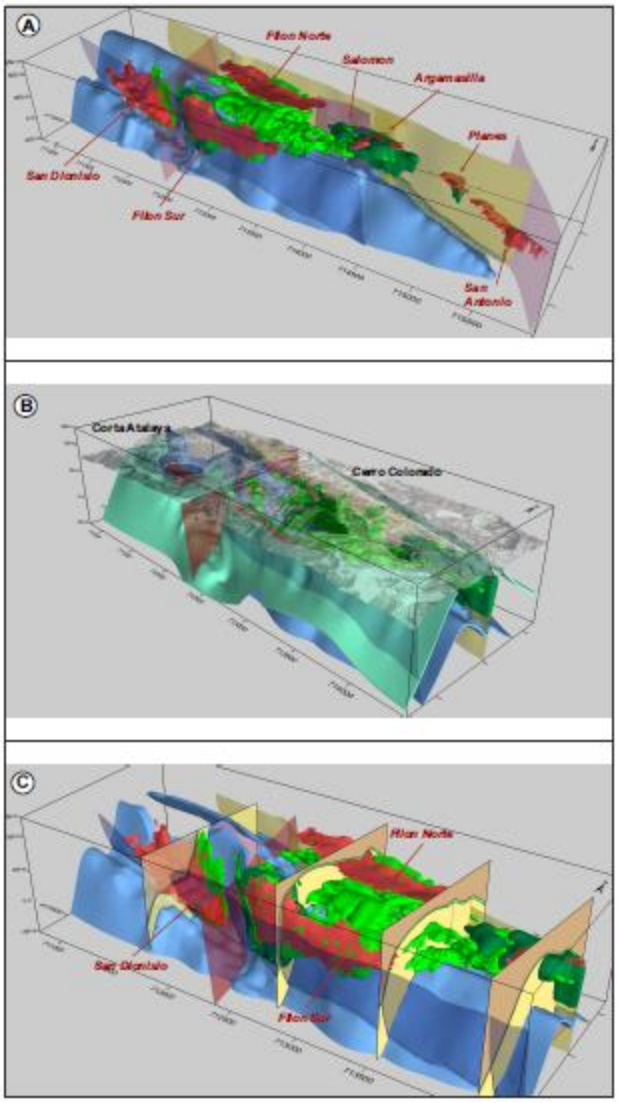

Figure 8

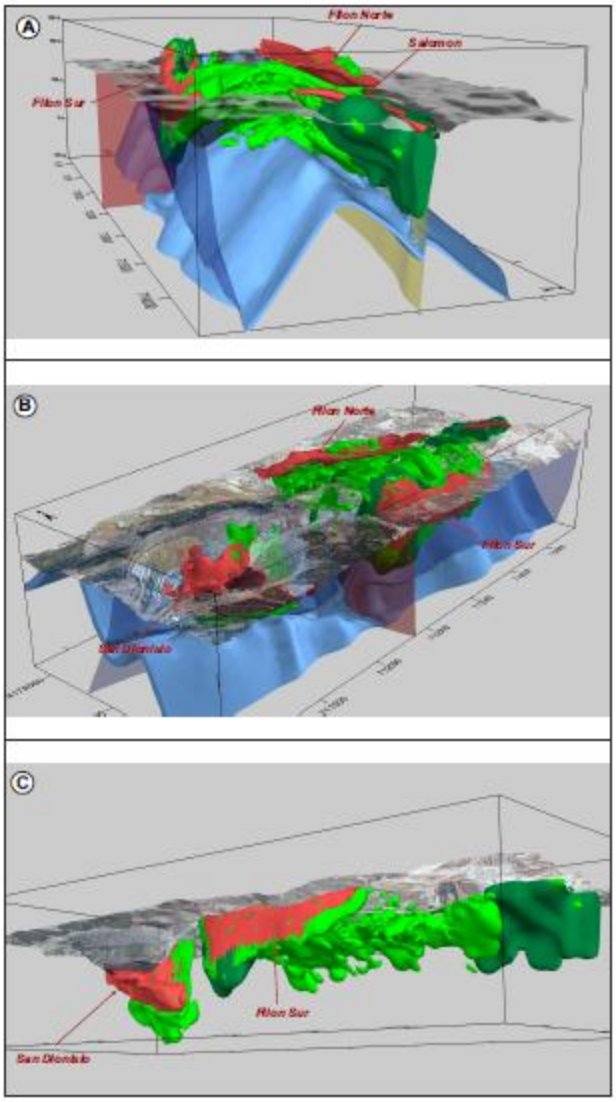

Figure 9

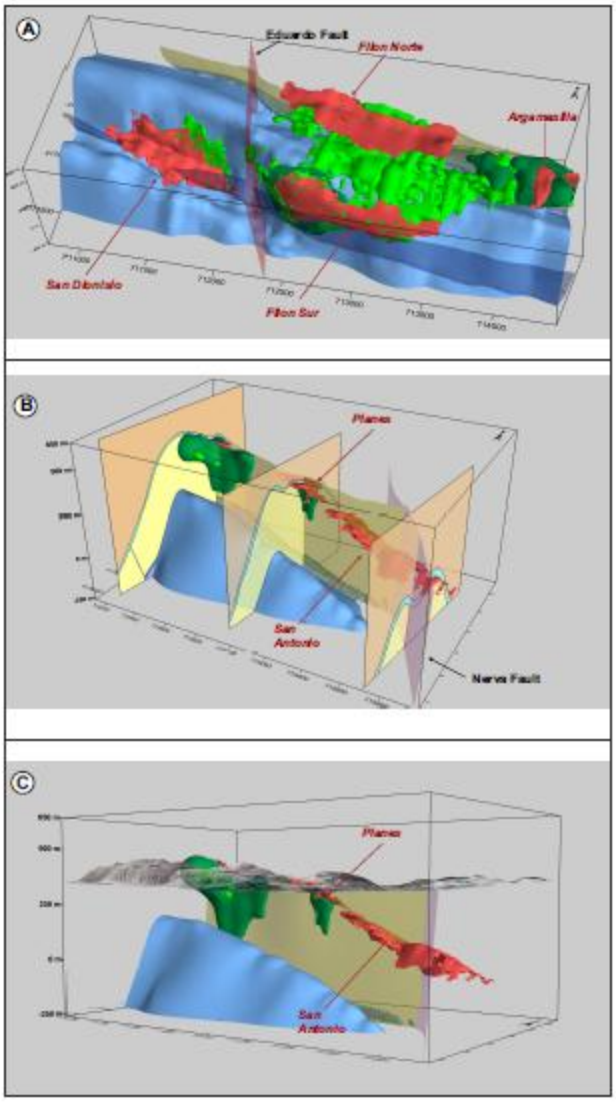

Figure 10

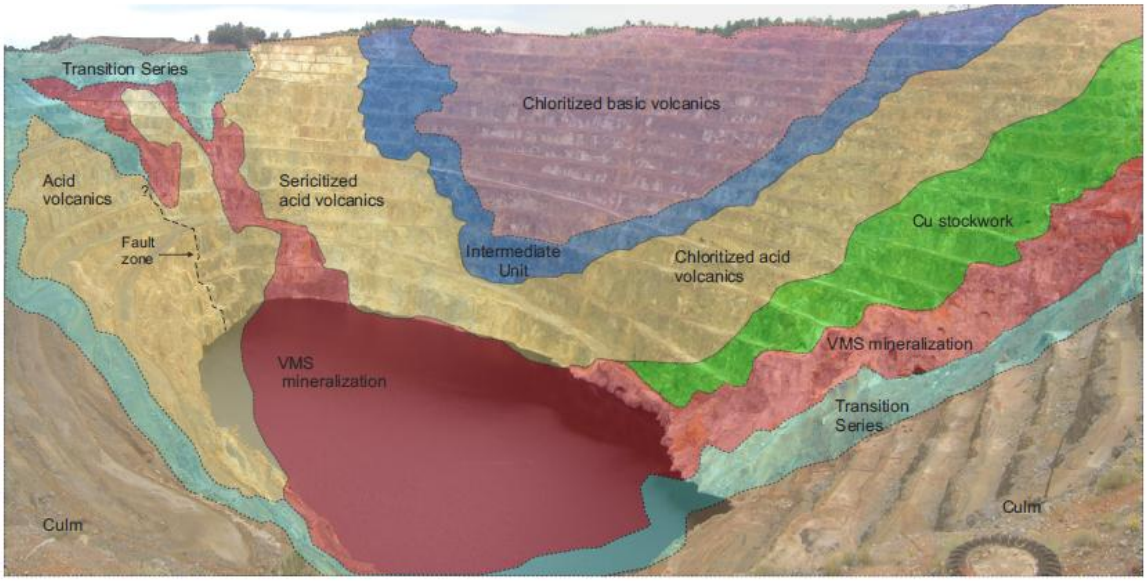

Figure 11

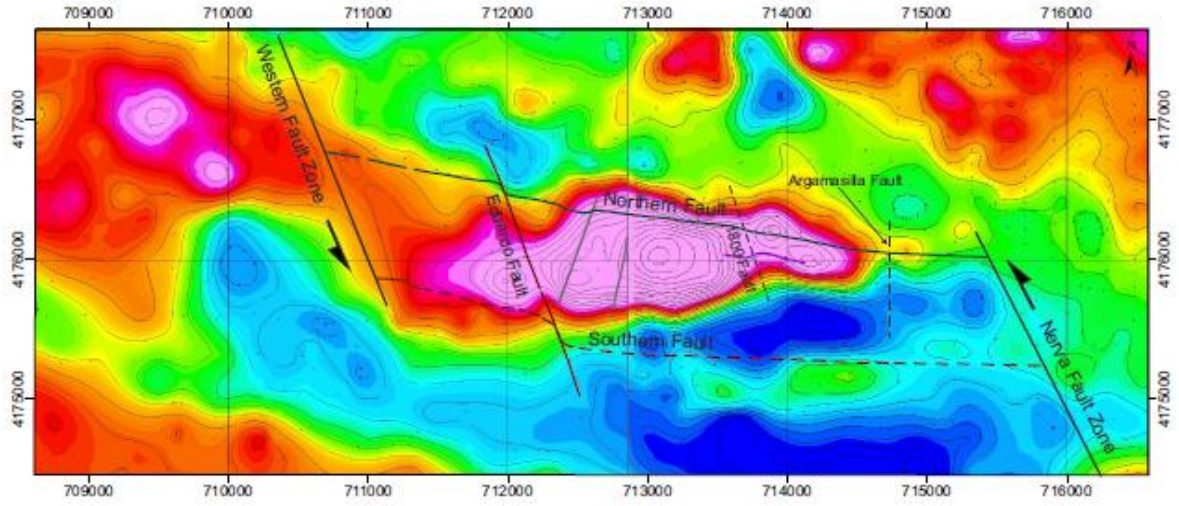

Figure 12

Figure 13

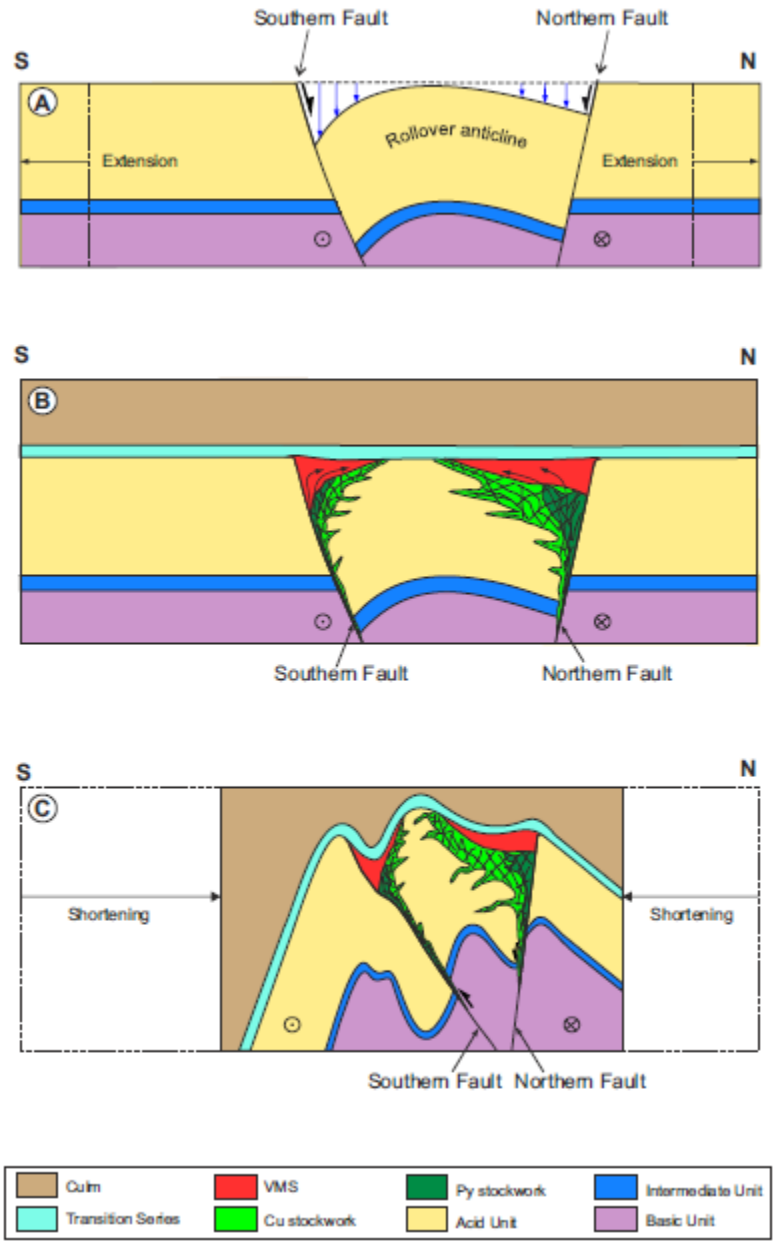

Figure 14

Figure 15

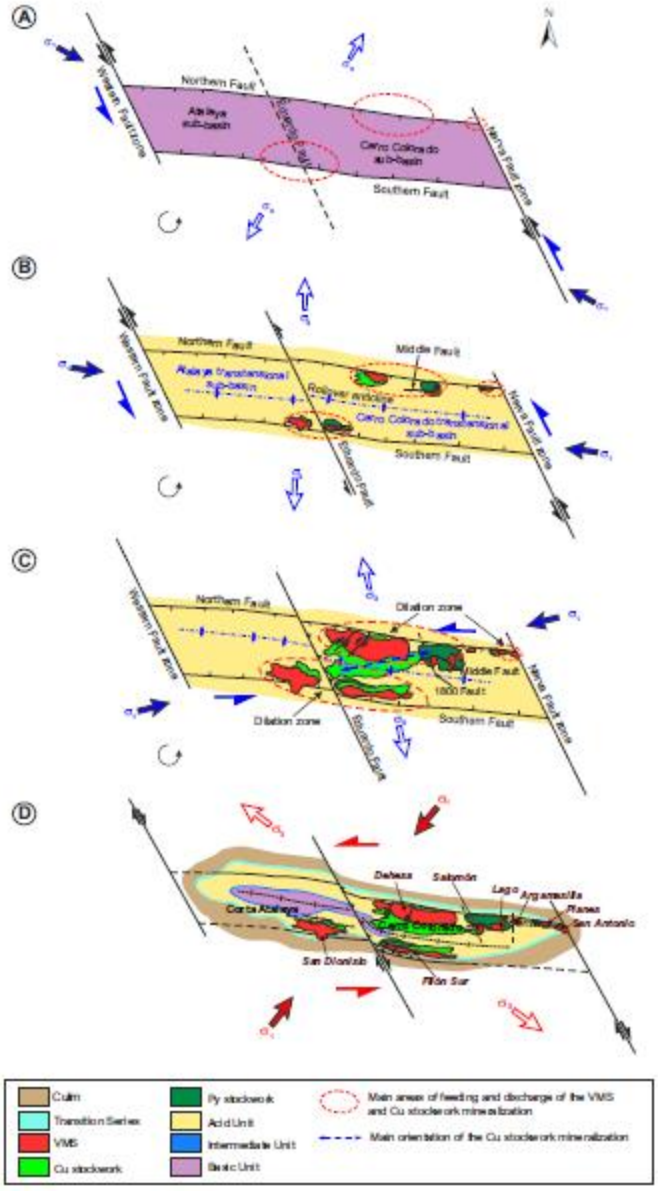

Figure 16

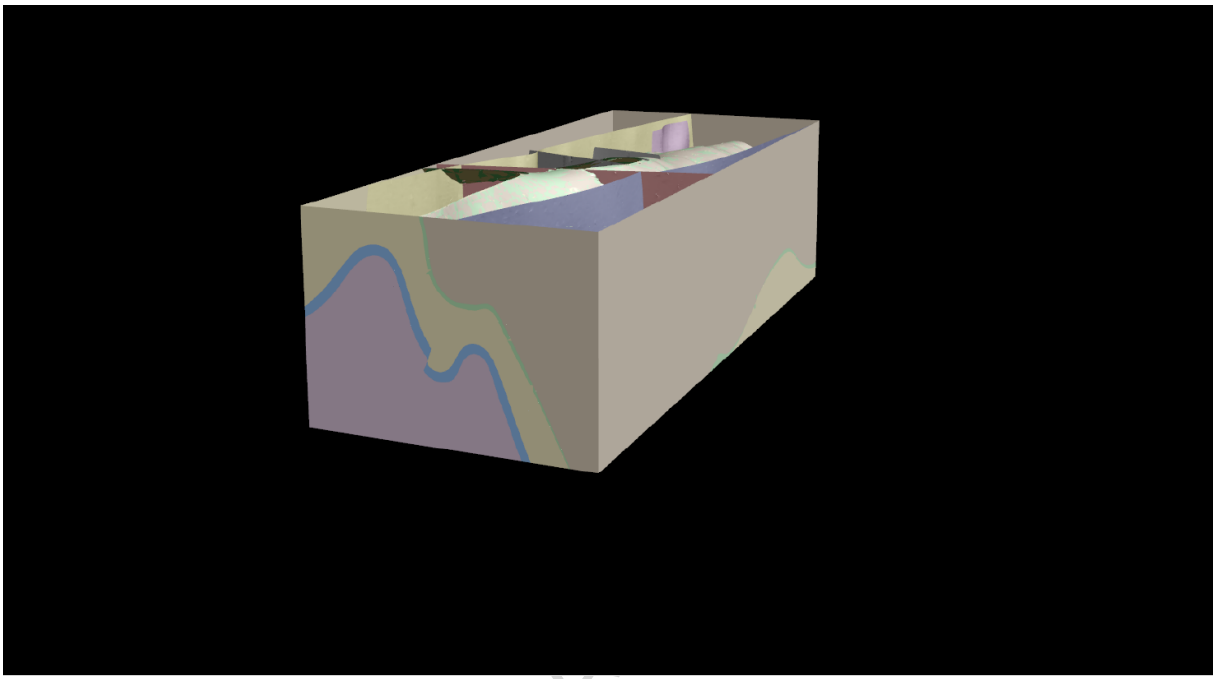

Appendix 1

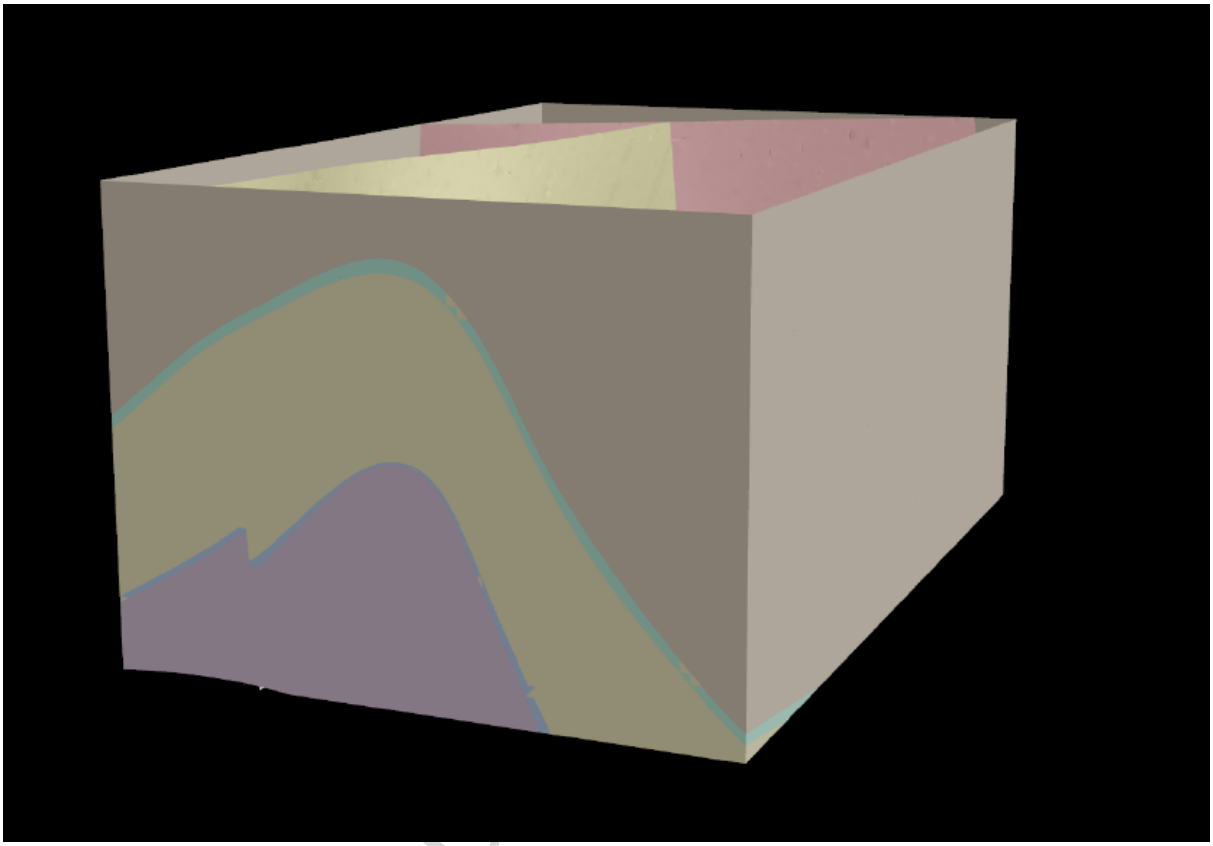

Appendix 2

Conflict of interest

There are two people who we would have scientific conflict of interests, Fernando Tornos (and his team of IGME), and Reinaldo Saez.

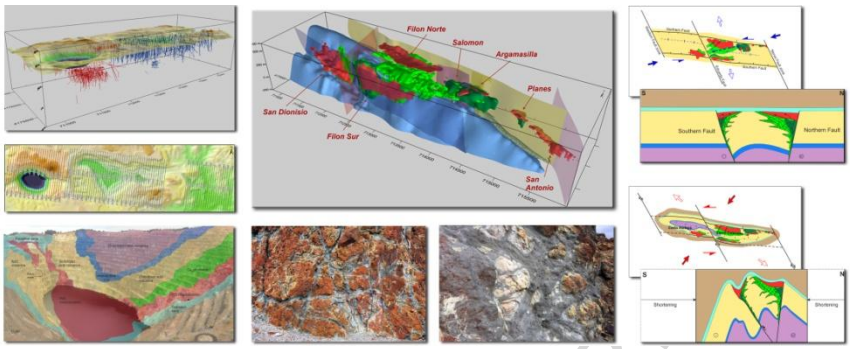

Graphical Abstract

Highlights

A new computer-generated 3D model of the Rio Tinto world class deposit is presented

We used data from 3,000 boreholes and 93 cross-sections for the 3D geological model

We emphasize on relationships between mineralization and transtensional pull-apart

A rollover anticline: a new structural model for the Rio Tinto district is presented

This new 3D model, based on real data, can be utilized for prospectivity in the IPB